Article

Metal Cation–Methyl Interactions in $CB_{11}Me_{12}^-$ Salts of MeGe, MeSn, and MePb

Ilya Zharov, Tsu-Chien Weng, Anita M. Orendt, Dewey H. Barich, James Penner-Hahn, David M. Grant, Zdenek Havlas, and Josef Michl

J. Am. Chem. Soc., **2004**, 126 (38), 12033-12046• DOI: 10.1021/ja0475205 • Publication Date (Web): 31 August 2004

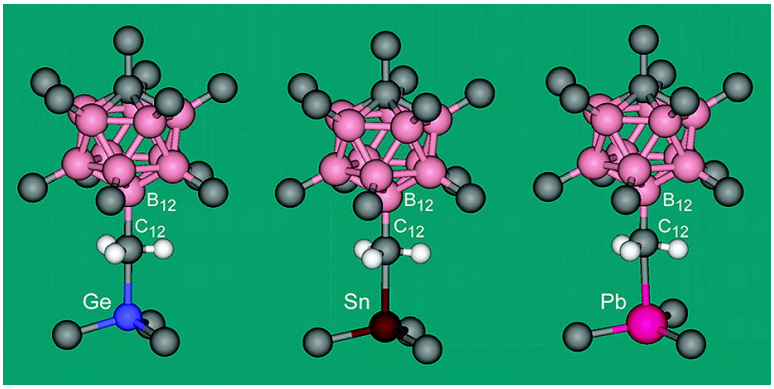

More About This Article

Additional resources and features associated with this article are available within the HTML version:

- Supporting Information
- Links to the 3 articles that cite this article, as of the time of this article download
- Access to high resolution figures
- Links to articles and content related to this article
- Copyright permission to reproduce figures and/or text from this article

View the Full Text HTML

J|A|C|S
ARTICLES
Published on Web 08/31/2004

Metal Cation−Methyl Interactions in $CB_{11}Me_{12}^-$ Salts of Me_3Ge^+, Me_3Sn^+, and Me_3Pb^+

Ilya Zharov,[†,⊥] Tsu-Chien Weng,[‡] Anita M. Orendt,[§] Dewey H. Barich,[§] James Penner-Hahn,[‡] David M. Grant,[§] Zdenek Havlas,[¶] and Josef Michl*[,†]

Contribution from the Department of Chemistry and Biochemistry, University of Colorado, Boulder, Colorado 80309-0215, Department of Chemistry, University of Utah, Salt Lake City, Utah 84112-0850, Department of Chemistry and Biochemistry, University of Michigan, Ann Arbor, Michigan 48109-1055, and Institute of Organic Chemistry and Biochemistry, Academy of Sciences of the Czech Republic, 16610 Prague 6, Czech Republic

Received April 28, 2004; E-mail: michl@eefus.colorado.edu

Abstract: Oxidation of Me_6M_2 (M = Ge, Sn) and Me_4Pb with the $CB_{11}Me_{12}^{\bullet}$ radical in alkane solvents produced the insoluble salts $Me_3M^+CB_{11}Me_{12}^-$, characterized by CP-MAS NMR and EXAFS. The cations interact with methyl groups of $CB_{11}Me_{12}^-$ with coordination strength increasing from Pb to Ge. Density functional theory (DFT) calculations for the isolated ion pairs, $Me_3M^+CB_{11}Me_{12}^-$ (M = Ge, Sn), revealed three isomers with the cation above methyl 2, 7, or 12, and not above a BB edge or a BBB triangle. The interaction has a considerable covalent component, with the cation attempting to perform a backside S_E2 substitution on the methyl carbon. In a fourth less favorable isomer the cation is near methyl 1, inclined toward methyl 2, and interacts with hydrogens. DFT atomic charge distributions and plots of the electrostatic potential on the surface of spheres centered at the $CB_{11}H_{12}^-$ and $CB_{11}Me_{12}^-$ icosahedra display the effects of uneven charge distribution within the anion and contradict the common belief that the negative charge of the cage anion is concentrated primarily on the cage boron atoms 7−12; in $CB_{11}Me_{12}^-$, roughly half is on the cage carbon and the rest on methyls 7−12.

Introduction

Coordination of methyl groups to metal cations is of considerable interest currently[1] because of its role in C−H activation[2] and in cation−anion interactions in transition metal catalysis.[3] Although some structures with a cationic transition metal coordinated to a methyl group are known,[4−9] examples of main group cations interacting with a methyl group are exceedingly rare.[10] Presently, we describe three new examples. An examination of the coordination of the weak ligand, a methyl group, to a cationic metal center poses two challenges. First, a cationic metal center such as R_3M^+ has to be made available, and second, counterions and solvents that would be stronger ligands than the methyl group must be absent.

The preparation and properties of the heavier congeners of carbenium ions, R_3M^+ (M = Si, Ge, Sn, Pb), in condensed media have been a subject of extensive studies and controversy for decades[11−13] because of fundamental interest in understanding similarities and differences between carbon and heavier group 14 elements. The obstacle hindering access to noncoordinated R_3M^+ cations is their extreme electrophilicity, which prevents the use of the usual fluoride-based superacids. In the presence of counterions or solvents, covalent bonds between the central atom of the R_3M^+ cation and the anion or the solvent are formed with extraordinary ease,[14−18] and very weakly nucleophilic anions[19] are required. Salts of simple noncoordinated group 14 cations such as R_3M^+ (R = H or alkyl)

[†] University of Colorado.
[‡] Unversity of Michigan.
[§] University of Utah.
[⊥] Present address: Department of Chemistry, University of Utah.
[¶] Academy of Sciences of the Czech Republic.

(1) Hall, C.; Perutz, R. N. *Chem. Rev.* **1996**, *96*, 3125 and references therein.
(2) Shilov, A. E.; Shul'pin, G. B. *Chem. Rev.* **1997**, *97*, 2879 and references therein.
(3) Marks, T. J.; Chen, E. Y.-X. *Chem. Rev.* **2000**, *100*, 1391 and references therein.
(4) Burns, C. J.; Andersen, R. A. *J. Am. Chem. Soc.* **1987**, *109*, 5853.
(5) Stults, S. D.; Andersen, R. A.; Zalkin, A. *J. Am. Chem. Soc.* **1989**, *111*, 4507.
(6) Berg, D. J.; Andersen, R. A. *Organometallics* **2003**, *22*, 627.
(7) Zhang, S.; Piers, W. E. *Organometallics* **2001**, *20*, 2088.
(8) Ingelson, M. J.; Mahon, M. F.; Patmore, N. J.; Ruggiero, G. D.; Weller, A. S. *Angew. Chem., Int. Ed.* **2002**, *41*, 3694.
(9) Clarke, A. J.; Ingleson, M. J.; Kociok-Köhn, G.; Mahon, M. F.; Patmore, N. J.; Rourke, J. P.; Ruggiero, G. D.; Weller, A. S. *J. Am. Chem. Soc.* **2004**, *126*, 1503.
(10) Zharov, I.; King, B. T.; Havlas, Z.; Pardi, A.; Michl, J. *J. Am. Chem. Soc.* **2000**, *122*, 10253.
(11) Lickis, P. D. In *The Chemistry of Organic Silicon Compounds*, 2nd ed.; Rappoport, Z., Apeloig, Y., Eds.; John Wiley & Sons: Chichester, UK, 1998; pp 557−594.
(12) Reed, C. A. *Acc. Chem. Res.* **1998**, *31*, 325.
(13) Zharov, I.; Michl. J. In *The Chemistry of Organic Germanium, Tin and Lead Compounds*; Rappoport, Z., Apeloig, Y., Eds.; Wiley & Sons: Chichester, 2002; Vol. 2, p 633.
(14) Ashradi, M.; Johnels, D.; Edlund, U. *Chem. Commun.* **1996**, 1279.
(15) Arshadi, M.; Johnels, D.; Edlund, U.; Ottosson, C.-H.; Cremer, D. *J. Am. Chem. Soc.* **1996**, *118*, 5120.
(16) Schleyer, P. v. R.; Buzek, P.; Müller, T.; Apeloig, Y.; Siehl, H.-U. *Angew. Chem., Int. Ed. Engl.* **1993**, *32*, 1471.
(17) Olah, G. A.; Rasul, G.; Prakash, G. K. S. *J. Organomet. Chem.* **1996**, *521*, 271.
(18) (a) Lambert, J. B.; Zhang, S.; Stern, C. L.; Huffman, J. C. *Science* **1993**, *260*, 1917. (b) Lambert, J. B.; Zhang, S.; Ciro, S. M. *Organometallics* **1994**, *13*, 2430.

have not been prepared and isolated, since suitable solvents and anions have not been found. Even *tert*-butyl groups fail to provide sufficient protection,[20] and only even more highly sterically hindered[21−25] and/or electronically stabilized[26−28] cations are known in non-coordinated form.[29] Although interesting in their own right, such highly hindered R_3M^+ cations are useless for the present purpose.

We use the salts $Me_3M^+CB_{11}Me_{12}^-$, in which the requisite methyl groups are carried by the anions, using alkanes as weakly coordinating solvents. This was suggested by the observations made on *n*-$Bu_3Sn^+CB_{11}Me_{12}^-$, which showed clear evidence of cation−methyl coordination.[10] The parent of the anion used is the deltahedral[30] carba-*closo*-dodecaborate(−) anion $CB_{11}H_{12}^-$ (**1**), whose substituted derivatives have received considerable attention recently.[19] The parent $CB_{11}H_{12}^-$ (**1**) was first synthesized by Knoth in 1967,[31] and is now accessible in two steps from cheap bulk chemicals, albeit in poor yield.[32] It contains a highly delocalized charge dispersed over a large icosahedral cage. It is inert to electrochemical oxidation in acetonitrile[33] and stable toward acids and bases. Its B−H bonds show distinct hydridic character,[34] and one can expect its halogenated[35] and methylated[36,37] derivatives to show some halide and methide anion character, and hence to have some coordinating ability as well. In this regard the trifluoromethylated derivative appears ideal, but unfortunately, it is shock-sensitive and explosive.[38] The $CB_{11}Me_{12}^-$ anion (**2**)[36] coordinates only weakly[39] and can only do so through its methyl groups. It has the additional advantage of carrying a lipophilic barrier around the carborane cage, alleviating possible solubility problems.[40] It is very stable toward bases and acids, except for neat strong acids such as hydrofluoric, sulfuric, triflic, and trifluoroacetic.[38]

The choice of a procedure for the generation of the $Me_3M^+CB_{11}Me_{12}^-$ salts poses an interesting challenge and is related to the choice of a reaction medium. For a long time, hydride abstraction by the trityl cation[41] provided the most successful way of generating group 14 cations in solution.[18,42] More recently, an alternative allyl leaving group approach was utilized to prepare trimesitylsilylium,[21] trimesitylgermylium,[43] and trimesitylstannylium[43] ions.[23] However, in both cases aromatic solvents appear to be the least coordinating media that can be used. To provide a reaction environment devoid of all unsaturation, we have taken advantage of a property of the $CB_{11}Me_{12}^-$ anion that can be viewed as its strong but also its weak point: it is much easier to oxidize than the parent $CB_{11}H_{12}^-$. The corresponding neutral radical $CB_{11}Me_{12}^{\bullet}$ (**3**)[39] is a stable one-electron oxidant that is freely soluble in nonpolar solvents. Its oxidation potential in acetonitrile, 1.15 V above the ferrocene/ferrocenium couple, is comparable to that of Ce(IV) at neutral pH.

Scheme 1

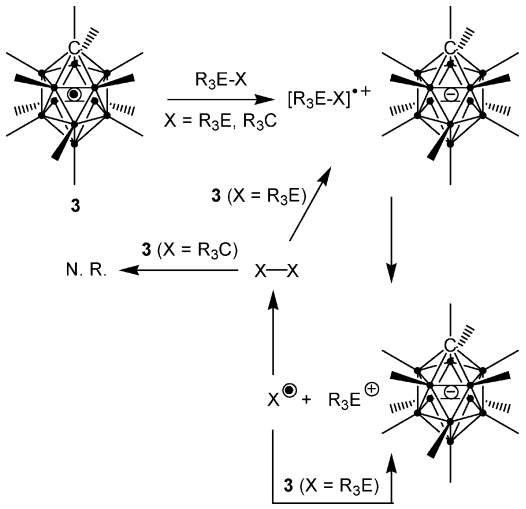

We use the radical **3** to prepare R_3M^+ cations by oxidation of neutral and nonpolar R_3M-containing precursors.[10] This reaction occurs even in highly nonpolar alkane solvents and simultaneously provides the desired R_3M^+ cation and the anion **2** (Scheme 1). The oxidation is believed to proceed in two single-electron-transfer steps. The first one would produce a cation radical from an $R_3M-M'R'_n$ precursor, whose weak one-electron bond could then dissociate to give the R_3M^+ cation and an $R'_nM'^{\bullet}$ radical. Depending on the nature of M′, the latter could be further oxidized in a second single-electron-transfer step to give the $R_3M'^+$ cation, or it could dimerize. Disproportionation is best avoided, since it produces unsaturated structures.

There is good precedent for the production of cations of group 14 elements by oxidation of neutral precursors. Recently, a series of complexes $[t\text{-}Bu_3M-N{\equiv}CR]^+$ (M = Si, Ge, Sn) has been prepared[44] by oxidation of the corresponding $t\text{-}Bu_6M_2$ dimetallanes with $Ph_3C^+B(3,5\text{-}CF_3\text{-}C_6H_3)_4^-$ in nitrile solvents. One-electron oxidation of Me_6Sn_2, $Me_3SnGeMe_3$, or $Me_3SnSiMe_3$ by the 10-methacridinium cation in acetonitrile led to the $[Me_3Sn-N{\equiv}CMe]^+$ cation.[45] Oxidation of R_4Sn, Me_3SnR, and

(19) (a) Lupinetti, A. J.; Strauss, S. H. *Chemtracts* **1998**, *11*, 565. (b) Reed, C. A. *Acc. Chem. Res.* **1998**, *31*, 133. (c) Krossing, I.; Raabe, I. *Angew. Chem., Int. Ed.* **2004**, *43*, 2066.
(20) Xie, Z.; Bau, R.; Benesi, A.; Reed, C. A. *Organometallics* **1995**, *14*, 3933.
(21) Lambert, J. B.; Zhao, Y. *Angew. Chem., Int. Ed. Engl.* **1997**, *36*, 400.
(22) Kim, K.-C.; Reed, C. A.; Elliott, D. W.; Mueller, L. J.; Tham, F.; Lin, L.; Lambert, J. B. *Science* **2002**, *297*, 825.
(23) Lambert, J. B.; Lin, L.; Keinan, S.; Muller, T. *J. Am. Chem. Soc.* **2003**, *125*, 6022.
(24) Sekiguchi, A.; Fukawa, T.; Lee, V. Y.; Nakamoto, M. *J. Am. Chem. Soc.* **2003**, *125*, 9250.
(25) Sekiguchi, A.; Fukawa, T.; Lee, V. Y.; Nakamoto, M.; Ichinohe, M. *Angew. Chem., Int. Ed.* **2003**, *42*, 1143.
(26) Sekiguchi, A.; Tsukamoto, M.; Ichinohe, M. *Science* **1997**, *275*, 60.
(27) Sekiguchi, A.; Matsuno, T.; Ichinohe, M. *J. Am. Chem. Soc.* **2000**, *122*, 11250.
(28) Sekiguchi, A.; Fukaya, N.; Ichinohe, M.; Ishida, Y. *Eur. J. Inorg. Chem.* **2000**, *6*, 1155.
(29) Sekiguchi, A.; Ichinohe, M.; Nakamoto, M. *Organometallic News* **2003**, *1*, 11.
(30) Grimes, R. N. *Carboranes*; Academic Press: New York & London, 1970.
(31) (a) Knoth, W. H. *J. Am. Chem. Soc.* **1967**, *89*, 1274. (b) Knoth, W. H. *Inorg. Chem.* **1971**, *10*, 598.
(32) Franken, A.; King, B. T.; Rudolph, J.; Rao, P.; Noll, B. C.; Michl, J. *Collect. Czech. Chem. Commun.* **2001**, *66*, 1238.
(33) Wiersema, R. J.; Hawthorne, M. F. *Inorg. Chem.* **1973**, *12*, 785.
(34) (a) Jelínek, T.; Plešek, J.; Heřmánek, S.; Štíbr, B. *Collect. Czech. Chem. Commun.* **1986**, *51*, 819. (b) Plešek, J.; Plzák, Z.; Stuchlík, J.; Heřmánek, S. *Collect. Czech. Chem. Commun.* **1981**, *46*, 1748.
(35) (a) Plešek, J. *Chem. Rev.* **1992**, *92*, 269. (b) Strauss, S. H. In *Contemporary Boron Chemistry*; Wade, K., Marder, T. B., Hughes, A., Eds.; Royal Society of Chemistry: London, 2000; Vol. 253, p 44. (c) Stasko, D.; Reed, C. A. *J. Am. Chem. Soc.* **2002**, *124*, 1148.
(36) King B. T.; Janoušek, Z.; Grüner, B.; Trammell, M.; Noll, B. C.; Michl, J. *J. Am. Chem. Soc.* **1996**, *118*, 3313.
(37) Clayton, J. R.; King, B. T.; Zharov, I.; Michl, J. Submitted for publication.
(38) King, B. T.; Michl, J. *J. Am. Chem. Soc.* **2000**, *122*, 10255.
(39) King, B. T.; Noll, B. C.; McKinley, A. J.; Michl, J. *J. Am. Chem. Soc.* **1996**, *118*, 10902.
(40) Pospíšil, L.; King, B. T.; Michl, J. *Electrochim. Acta* **1998**, *44*, 103.
(41) Corey, J. Y. *J. Am. Chem. Soc.* **1975**, *97*, 3237.
(42) Xie, Z.; Manning, J.; Reed, R. W.; Mathur, R.; Boyd, P. D.; Benesi, A.; Reed, C. A. *J. Am. Chem. Soc.* **1996**, *118*, 2922.
(43) Lambert, J. B.; Zhao, Y.; Wu, H.; Tse, W. C.; Kuhlman, B. *J. Am. Chem. Soc.* **1999**, *121*, 5001.
(44) Ichinohe, M.; Fukui, H.; Sekiguchi, A. *Chem. Lett.* **2000**, *12*, 600.
(45) Fukuzumi, S.; Kitano, T.; Mochida, K. *J. Am. Chem. Soc.* **1990**, *112*, 3246.

R_6Sn_2 (R = Me, Et, *n*-Bu, Ph, vinyl) by the thianthrene cation radical in acetonitrile also resulted in the formation of the corresponding $[R_3Sn{-}N{\equiv}CMe]^+$ cations,[46] and the $[Ph_3Pb{-}N{\equiv}CMe]^+$ cation was prepared by oxidation of Ph_6Pb_2 with $AgNO_3$ in acetonitrile.[47] Electrooxidation of various organotin and organolead compounds has been shown to proceed via electron transfer as the rate-determining step and to first produce the cation radicals $[R_3M\text{-}MR_3]^{\bullet+}$, which then decompose to give R_3M^+ and $R_3M^\bullet$, followed by further radical oxidation.[48] One-electron oxidation of the highly hindered stable stannyl radical $(t\text{-}Bu_2MeSi)_3Sn^\bullet$ yielded the stable cation $(t\text{-}Bu_2MeSi)_3Sn^+$.[24]

The next issue is the solubility of the resulting salt in the alkane solvent, critical if single crystals are to be grown. In a short communication, we reported that the use of *n*-butyl substituents provides sufficient solubility for crystallization of the resulting salt, $n\text{-}Bu_3Sn^+CB_{11}Me_{12}^-$, from hexane.[10] Presently, however, we deal with the $CB_{11}Me_{12}^-$ salts of the simplest trialkylated cations, Me_3E^+, accessed by applying the reaction of Scheme 1 to Me_6Ge_2, Me_6Sn_2, and Me_4Pb. In this case, the lower solubility in alkanes prevented us from obtaining single crystals, and we had to resort to powder EXAFS measurements to obtain structural information. The results obtained from the reaction of **3** with Me_6Si_2 were different in that **3** acted as a methyl radical transfer agent rather than an electron transfer agent, and they will be reported separately.[49]

Results and Discussion

Preparation and NMR Spectra of $Me_3Sn^+CB_{11}Me_{12}^-$ (4). When a solution of 1 equiv of hexamethyldistannane (Me_6Sn_2) in dry pentane was added to a solution of 2 equiv of the radical **3** in dry pentane at −78 °C under argon atmosphere, the blue color of the radical disappeared within seconds and a white solid **4** formed. This was soluble in polar solvents. The ^{11}B NMR spectrum of its acetone solution was identical to that of the Cs^+ salt of the anion **2**. Negative-mode ES/MS of its methanol solution showed a single anion with *m*/*e* 311 (both *m*/*e* and isotopic distribution identical to those of the anion **2**), while positive-mode ES/MS of the same solution showed a cation with *m*/*e* 165 and isotopic distribution characteristic of compounds with a single Sn atom in the molecule. This corresponds to the Me_3Sn^+ cation. In acetonitrile, several complexes of the type $[Me_3Sn(CH_3CN)_m(H_2O)_n]^+$ were found in the mass spectrum. Such behavior of R_3Sn^+ cations under atmospheric pressure ionization/electrospray conditions has been reported.[50] All this suggested that **4** indeed was the desired $Me_3Sn^+CB_{11}Me_{12}^-$ salt (Scheme 2).

This conclusion was further verified by a reaction of **4** with PhLi in pentane (Scheme 2), which yielded two products. A pentane-soluble product was isolated by preparative GC in 95% yield based on Me_6Sn_2. Its NMR and GC/MS spectra were identical with those of an authentic sample of Me_3SnPh and agreed with published reports.[51] The pentane-insoluble product was identified by NMR and ES/MS as Li^+**2**.

Scheme 2

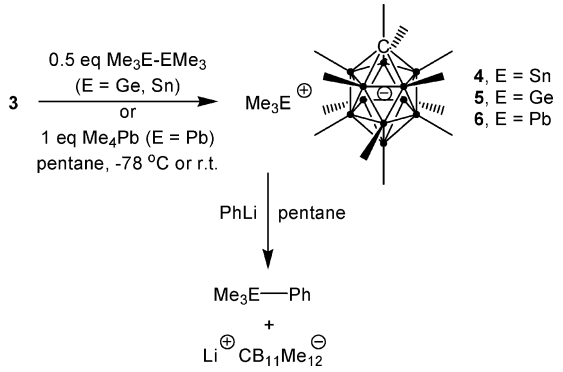

The white solid **4**, obtained in pentane at −78 °C, was dissolved in dry C_6D_6, and then the solution was frozen in liquid nitrogen and transported to an NMR instrument. An ^{119}Sn NMR spectrum was taken as soon as the solvent in the NMR tube melted and showed a ^{119}Sn NMR signal at 324.7 ppm. The benzene solution of **4** was not stable upon warmup and darkened ca. 10 min after reaching room temperature. Numerous ^{119}Sn NMR signals at lower chemical shifts were then observed, together with a clean ^{11}B NMR spectrum of **2**, which suggests that the benzene adduct of the Me_3Sn^+ cation decomposed, leaving the anion **2** intact. This was confirmed by the negative-mode ES/MS of the resulting solution, which showed only the presence of **2**.

A similar experiment with CD_2Cl_2 at −60 °C yielded a solution that gave a ^{119}Sn NMR spectrum with a signal at 335.9 ppm and a ^{11}B NMR spectrum with signals at −1.96 (1 B) and 9.20 (10 B, unresolved), similar to those of **2**. When the temperature was raised from −60 to 0 °C, the signals of B_{7-11} and B_{2-6} became resolved, which suggests that at the lower temperature the interaction of the Me_3Sn^+ cation and the anion **2** is stronger than the interaction of the cation with the solvent, while at higher temperature this order is reversed. The CD_2Cl_2 solution of **4** was again unstable above 0 °C.

The ^{119}Sn NMR shifts found for **4** in C_6D_6 and CD_2Cl_2 are similar to (a) the signal at 348 ppm reported[52] for $n\text{-}Bu_3Sn^+\text{-}B[3,5\text{-}(F_3C)_2\text{-}C_6H_3]_4^-$ in CD_2Cl_2 at −70 °C (this signal disappeared above −20 °C); (b) the signal at 360 ppm reported[53] for $n\text{-}Bu_3Sn^+[B(C_6F_5)_3H]^-$ in C_6D_6; and (c) the signal at 322 ppm reported[54] for $Me_3Sn^+SO_3F^-$ in HSO_3F at −60 °C. They are somewhat lower than the 434.2 ppm reported[55] for $Bu_3Sn^+\text{-}[B(C_6F_5)_4]^-$ in toluene-d_8 and the 434 ppm reported[56] for $Bu_3Sn^+[C_6F_4\text{-}1,2\text{-}\{B(C_6F_5)_2\}_2(\mu\text{-}OCH_3)]^-$ in toluene-d_8.

When dissolved in CD_3CN at −40 °C, the white solid **4** gave a ^{119}Sn NMR signal at 233.1 ppm and ^{11}B NMR signals at −1.07 (1 B), −8.97 (5 B), and −10.86 (5 B). This solution was unstable above −5 °C. The large displacement of ∼ −100 ppm in the ^{119}Sn NMR signal of **4** in CD_3CN demonstrates that the interaction of Me_3Sn^+ with the solvent is quite strong, while ^{11}B NMR shows no interaction with the anion. When a small amount of water was added to this solution, a new signal at 205.0 ppm appeared, similar to that reported[57] for $(Et_3Sn)_2O^+H$ in C_6D_6.

(46) Loczynski, S.; Boduszek, B.; Shine, H. J. *J. Org. Chem.* **1991**, *56*, 914.
(47) Doretti, L.; Faleschini, S. *Gazz. Chim. Ital.* **1970**, *100*, 819.
(48) Kochi, J. K. *Angew. Chem., Int. Ed. Engl.* **1988**, *27*, 1227.
(49) Zharov, I.; Fete, M. G.; Michl, J. Unpublished results.
(50) Dakternieks, D.; Lim, A. E. K.; Lim, K. F. *Phosphorus, Sulfur, Silicon Relat. Elem.* **1999**, *150−151*, 339. (b) Henderson, W.; Taylor, M. J. *Polyhedron* **1996**, *15*, 1957.
(51) Bullpitt, M.; Kitching, W.; Adcock, W. *J. Organomet. Chem.* **1976**, *116*, 161.
(52) Kira, M.; Oyamada, T.; Sakurai, H. *J. Organomet. Chem.* **1994**, *471*, C4.
(53) Lambert, J. B.; Kuhlmann, B. *J. Chem. Soc., Chem. Commun.* **1992**, 931.
(54) Birchall, T.; Manivannan, V. *J. Chem. Soc., Dalton Trans.* **1985**, 2671.
(55) Blackwell, J. M.; Piers, W. E.; McDonald R. *J. Am. Chem. Soc.* **2002**, *124*, 1295.
(56) Henderson, L. D.; Piers, W. E.; Irvine, G. J.; McDonald, R. *Organometallics* **2002**, *21*, 340.

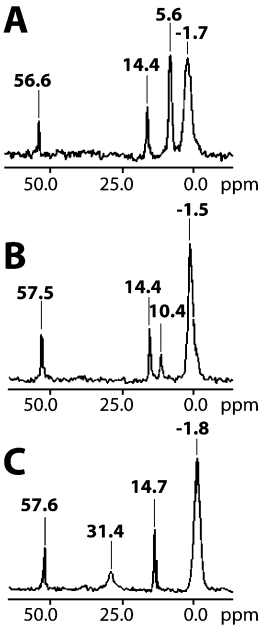

Figure 1. CP-MAS ^{13}C NMR of (A) $Me_3Ge^+CB_{11}Me_{12}^-$ (**5**), (B) $Me_3Sn^+CB_{11}Me_{12}^-$ (**4**), and (C) $Me_3Pb^+CB_{11}Me_{12}^-$ (**6**).

The CP-MAS ^{11}B NMR spectrum of solid **4** was identical to that of Cs^+**2**. CP-MAS ^{13}C NMR of **4** (Figure 1B) confirmed the presence of $CB_{11}Me_{12}^-$ and was compatible with the presence of Me_3Sn^+. The signal of the Me_3Sn^+ carbon in **4** at 10.4 ppm is at higher chemical shift relative to the signals of the C_α−Sn carbon in neutral tin compounds (cf. −9 ppm for Me_4Sn, 0.3 ppm for Me_3SnCl[58]), which is compatible with the presence of positive charge on the Sn atom, in agreement with the ^{119}Sn NMR chemical shift. We realize that other factors may dominate the chemical shift value, in particular the decreased excitation energies in the cation.

The CP-MAS ^{119}Sn NMR signal for solid **4** was found at 466.2 ppm. While this number is higher than those observed for the complexes of **4** in solution, it is much lower than the 806 ppm chemical shift reported[43] for the Mes_3Sn^+ cation, and particularly the 2653 ppm shift reported[24] for the non-coordinated tin atom in $(t\text{-}Bu_2MeSi)_3Sn^+B(C_6F_5)_4^-$. Clearly, the Me_3Sn^+ cation in solid **4** is significantly coordinated, and the only coordination possible is to the methyl groups of the anion. Unfortunately, CP-MAS NMR did not reveal any changes in the chemical shifts of either methyl group carbons or cage boron atoms of the anion that would provide further evidence for this coordination.

Et_4Sn was also tested as a precursor for a trialkylstannylium ion. Its reaction with the radical **3** is slower and not as clean as in the case of Me_6Sn_2 but does result in $Et_3Sn^+CB_{11}Me_{12}^-$, as judged by ES/MS.

Preparation and NMR Spectra of $Me_3Ge^+CB_{11}Me_{12}^-$ (5). An analogous oxidation of 1 equiv of hexamethyldigermane (Me_6Ge_2) with 2 equiv of the radical **3** in dry pentane at room temperature produced a white solid **5** within 1 h. The ^{11}B NMR spectrum of its acetone solution was identical to that of the Cs^+ salt of the anion **2**. Negative-mode ES/MS of its methanol solution showed only the anion **2**, while positive-mode ES/MS of the products showed $[(Me_3Ge)_2OH]^+$ and Me_3Ge^+ cations. Reaction of the white precipitate **5** with PhLi in pentane (Scheme 2) yielded Me_3GePh (89% yield based on Me_6Ge_2, isolated by preparative GC; NMR and MS spectra identical to those reported[59]) and Li^+**2** (by NMR and ES/MS). All this suggested that **5** is the anticipated $Me_3Ge^+CB_{11}Me_{12}^-$ salt (Scheme 2).

Germanium lacks a sensitive and convenient NMR nuclide,[60] and there is no easy direct NMR method to confirm the formation of Me_3Ge^+ in the above reaction by dissolving **5** in a way similar to that described for **4**, or in the solid state. The CP-MAS ^{11}B NMR spectrum of **5** was identical to that of Cs^+**2**. The CP-MAS ^{13}C NMR spectrum of **5** (Figure 1A) was compatible with the presence of Me_3Ge^+, and neither of these spectra showed direct evidence for a coordinating interaction. The ^{13}C signal of Me_3Ge^+ at 5.6 ppm is at higher chemical shift relative to the signals of C_α−Ge in neutral germanium compounds (cf. −1 ppm in Me_4Ge, −1.7 ppm in Me_3GeCN[59]), compatible with the presence of positive charge on the Ge atoms. It is at lower chemical shift from the corresponding signal for Me_3Sn^+ (10.4 ppm), suggesting that the positive charge on the Ge atom in **5** is smaller than that on the Sn atom in **4**, and that the cation−anion charge-transfer interactions in **5** are stronger than those in **4**. However, the difference could also be due to increased bond strengths and higher excitation energies in Me_3Ge^+ compared to Me_3Sn^+.

The reaction of Et_4Ge with the radical **3** is much slower than the reaction of Me_6Ge_2 but still results in $Et_3Ge^+CB_{11}Me_{12}^-$ (as determined by ES/MS).

Preparation and NMR Spectra of $Me_3Pb^+CB_{11}Me_{12}^-$ (6). Hexamethyldiplumbane ($Me_3Pb-PbMe_3$) can be prepared relatively easily[61] but is unstable and readily decomposes after preparation, or upon storing even in the absence of air. Since it was possible to oxidize Et_4Sn and Et_4Ge with the radical **3**, oxidation of tetramethylplumbane (Me_4Pb), which is a stable compound at room temperature (but can spontaneously detonate during a distillation[62]), was attempted. When 1 equiv of tetramethylplumbane (Me_4Pb) in dry pentane was treated with 1 equiv of the radical **3** in dry pentane at −78 °C, the blue color of the radical disappeared within seconds, and a white solid **6** was formed. ^{11}B NMR and negative-mode ES/MS of its acetone solution clearly showed that the anion **2** was formed as the only boron-containing product in the above reaction. In addition, positive-mode ES/MS of its methanol solution showed the Me_3Pb^+ cation.

Reaction of the white precipitate **6** with PhLi in pentane yielded Me_3PbPh (89% yield based on Me_4Pb, isolated by preparative GC; NMR and MS spectra were identical to those reported[51]) and Li^+**2** (by NMR and ES/MS). All this suggested that **6** was the hoped-for $Me_3Pb^+CB_{11}Me_{12}^-$ (Scheme 2).

The white solid **6** obtained in pentane was not soluble in C_6D_6 but dissolved in dry CD_2Cl_2. This solution, stable at room temperature, showed a ^{207}Pb NMR signal at 1007.4 ppm and ^{11}B NMR signals at −0.99 (1 B), −8.37 (5 B), and −9.79 (5 B), similar to those of the Cs^+ salt of the anion **2**. The ^{207}Pb

(57) Lambert, J. B.; Ciro, S. M.; Stern, C. L. *J. Organomet. Chem.* **1995**, *499*, 49.
(58) Mann, B. E.; Taylor, B. F. *^{13}C NMR Data for Organometallic Compounds*; Academic Press: London, 1981; pp 64−77.
(59) Neumann, W. P.; Kuehlein, K. *Justus Liebigs Ann. Chem.* **1967**, *702*, 13.
(60) Harris, R. K. In *NMR and Periodic Table*; Harris, R. K., Mann, B. E., Eds.; Academic Press: London, 1978; p 7.
(61) Arnold, D. P.; Wells, P. R. *J. Organomet. Chem.* **1976**, *111*, 269.
(62) .Gilman, H.; Jones, R. G. *J. Am. Chem. Soc.* **1950**, *72*, 1760.

NMR shift found for **6** in CD_2Cl_2 is similar to the signal at 980 ppm reported[14] for $Me_3Pb^+SO_3F^-$ in HSO_3F at low temperature.

Although it is relatively easy to observe ^{207}Pb NMR in solution,[63] CP-MAS ^{207}Pb NMR experiments can be quite demanding,[64] and for **6** they have failed. At the same time, the ^{13}C and ^{11}B CP-MAS NMR spectra of **6** were measured successfully. The CP-MAS ^{11}B NMR spectrum of **6** was identical to that of Cs^+**2**. The CP-MAS ^{13}C NMR spectrum of **6** (Figure 1C) confirmed the presence of $CB_{11}Me_{12}^-$ and was compatible with the presence of Me_3Pb^+. Neither spectrum showed any direct evidence for a coordinating interaction. The ^{13}C signal of Me_3Pb^+ at 31.4 ppm is at a significantly higher chemical shift than the signals of the C_α–Pb carbon in neutral lead compounds (cf. −3 ppm in Me_4Pb, 15.2 ppm in Me_3PbBr)[59] and also from the corresponding signal for Me_3Sn^+ (10.4 ppm), compatible with the notion that the positive charge on the Pb atom in **6** is larger compared to that on the Sn atom in **4**, and that the cation–anion charge-transfer interactions in **6** are weaker than those in **4**. Once again, it is possible that the sources of the differences are the weaker C–Pb bonds and the lower excitation energies in Me_3Pb^+.

The EXAFS Structure of the $Me_3M^+CB_{11}Me_{12}^-$ Solids (4–6). Our attempts to grow crystals of **4**, **5**, and **6** from alkane solvents failed due to the insufficient solubility of these compounds. Attempts to use slow diffusion of reagents also failed, and powder diffraction[65] showed that all the solids obtained were predominantly amorphous. Structural information was, however, obtained from extended X-ray absorption fine structure (EXAFS) analysis. The refinement procedure was first calibrated on the tetraphenyl compounds Ph_4M (M = Ge, Sn, Pb). In each case, the C–M distance determined by EXAFS agreed within 0.002 Å with that deduced from single-crystal X-ray diffraction (Table S2, Supporting Information).[66]

The Fourier transforms of the EXAFS data for **4**, **5**, **6**, and the Ph_4M references are shown in Figure 2, and the EXAFS data are included in the Supporting Information (Figure S1). The best fits to the EXAFS data are summarized in Table 1.

Two sets of M–C distances, a short one and a long one, were found by EXAFS of **4**, **5**, and **6**. The first-shell peak is assigned to the methyl carbon directly attached to the metal. As expected, it moves progressively to longer distance on going from Ge to Sn and to Pb (1.94, 2.12, and 2.17 Å, respectively; see Tables 1 and S2). This $M-C_\alpha(sp^3)$ distance is approximately 0.02 Å shorter than the $M-C_\alpha(sp^2)$ distances in the corresponding Ph_4M compounds, and about 0.04 Å shorter than a normal $M-C_\alpha(sp^3)$ bond (1.98, 2.14, and 2.22 Å, respectively[67]), as would be expected for a metal atom hybridization close to sp^2. Although this difference is small, previous studies have shown that the precision of EXAFS is typically 0.004 Å.[68] Therefore, given the availability of excellent reference compounds, we are confident that this represents a real decrease in the $M-C_\alpha$ distance.

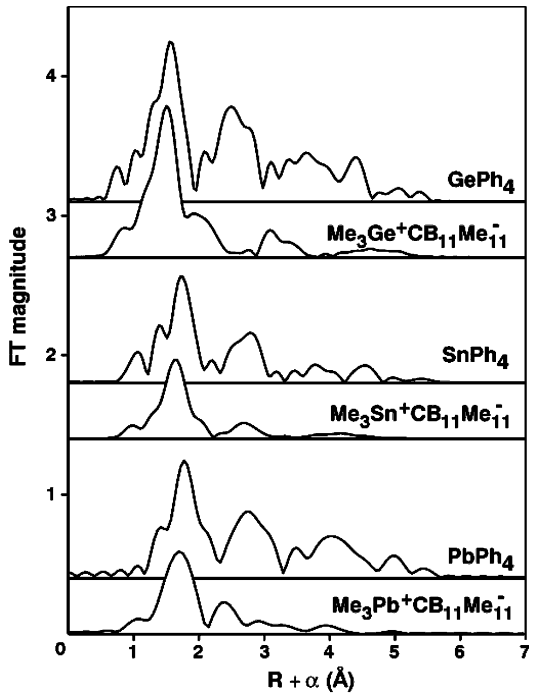

Figure 2. Fourier transforms of the k^3-weighted EXAFS data for **4**, **5**, and **6**. All spectra are plotted on the same scale and offset vertically for clarity. Fourier transforms were calculated over the range 2–15 $Å^{-1}$ for **4** and **5** and 2–10 $Å^{-1}$ for **6**. For each element, data for Ph_4E (pronounced outer-shell scattering) and $Me_3E^+CB_{11}Me_{12}^-$ are paired to emphasize the difference in outer-shell scattering.

Table 1. Structural Data (Å, $Å^2$, deg) from EXAFS of Solid **4**, **5**, and **6**, and as Calculated[a] for Isolated $Me_3M^+CB_{11}Me_{12}^-$ Ion Pairs Coordinated in Position 12 of $CB_{11}Me_{12}^-$

		M		
		Ge[b]	Sn	Pb
d(M–C_α)	EXAFS	1.94	2.12	2.17
	$\sigma^2 \times 10^3$	1.6	2.4	3.8
	calcd	1.98 (1.95)	2.15	2.18
d(M···C)	EXAFS	2.49	2.77, 3.02	2.9
	$\sigma^2 \times 10^3$	3	3	8
	calcd	2.14 (2.10)	2.42	2.63
d(M···X)[c]	EXAFS	3.63	4.63	4.51
	$\sigma^2 \times 10^3$	2.6	5.2	6.6
calcd d[C(12)···B(12)]		1.85 (1.75)	1.72	1.67
calcd ⟨d[M···C(7,8)]⟩		5.07 (4.81)	5.22	5.24
calcd ⟨d[M···C(7,8)]⟩		4.42 (4.11)	4.54	4.35
calcd $\angle B_{12}C_{12}M$		180 (171)	180	173
calcd $\sum\angle C_\alpha MC_\alpha$		340 (342)	347	354
calcd ⟨∠BCH⟩		86 (90)	96	101

[a] B3LYP/SDD. [b] MP2/6-31G(d) results in parentheses. [c] An outer-shell distance.

In all cases, there is clear evidence of additional outer-shell scattering, indicative of M···C interactions, for which the EXAFS distance determinations will be less accurate. For the tetraphenyl species, the outer-shell scattering is readily understood as arising from the phenyl carbons located farther than the ipso carbon. Fits to these data require the use of multiple-scattering corrections. Data fits obtained by constraining the phenyl ring to the known geometry and allowing only M···C distances and Debye–Waller factors to vary were in excellent

(63) Wrackmeyer, B.; Horchler, K. In *Annual Reports on NMR Spectroscopy*; Webb, G. A., Ed.; Academic Press: London, 1990; Vol. 22, pp 249–250.
(64) Sebald, A. In *Advanced Applications of NMR to Organometallic Chemistry*; Gielen, M., Willem, R., Wrackmeyer, B., Eds.; Wiley & Sons: Chichester, UK, 1996; pp 124–157.
(65) Performed by Prof. Peter W. Stephens at the State University of New York, Stony Brook, NY.
(66) (a) Chieh, P. C. *J. Chem. Soc. A* **1971**, 3243. (b) Belsky, V. K.; Simonenko, A. A.; Reikhsfeld, V. O.; Saratov, I. E. *J. Organomet. Chem.* **1983**, *244*, 125. (c) Preut, H.; Huber, F. *Acta Crystallogr. C* **1993**, *49*, 1373.
(67) Allen, F. H.; Kennard, O.; Watson, D. G.; Brammer, L.; Orpen, A. G.; Taylor, R. *J. Chem. Soc., Perkin. Trans 2* **1987**, S1.
(68) Riggs-Gelasco, P. J.; Mei, R.; Ghanotakis, D. F.; Yocum, C. F.; Penner-Hahn, J. E. *J. Am. Chem. Soc.* **1996**, *118*, 2400.

agreement with crystallographic data and provided confidence that the outer-shell fits for the carboranyl salt data should also be reliable.

For all three cations, the longer M···C distances (2.5−3.0 Å) can only be interpreted as the distance between the Me_3M^+ cation and the carbon atom of a methyl group of the $CB_{11}Me_{12}^-$ anion with which the cation interacts. These distances are longer than the normal M−C bond lengths but are much shorter than the sum of van der Waals radii of Ge (2.0 Å[69]), Sn (2.17 Å[70]), or Pb (2.2 Å[71]) and of a methyl group (2.0 Å[69]). Clearly, the cation−anion interactions in **4**, **5**, and **6** are significant. We shall see below that this is further supported by the observation of features attributable to M···C−B scattering in **4** and **6**, and by the observation of a further outer-shell Ge···C scattering in **5** that must arise from an additional cation−anion interaction.

EXAFS of Solid $Me_3Sn^+CB_{11}Me_{12}^-$ (4) and $Me_3Pb^+CB_{11}Me_{12}^-$ (6). The first of the two outer-shell peaks seen for the Sn atom in **4** and the Pb atom in **6** is much more intense than the second. For **4**, the data can be fitted using a single outer-shell distance of approximately 3.03 Å, with an additional weak peak at $R + \alpha \approx 4.1$ Å that can be modeled as the scattering from the B atom in a linear Sn···CH_3−B unit (α is the "EXAFS phase shift", whose typical magnitude is 0.4 Å). Although the $R + \alpha \approx 4.1$ Å peak is weak and the Sn···B distance thus is not well defined, the apparent Sn···B distance of 4.63 Å would be consistent with a quite reasonable C−B distance of 1.60 Å.

However, closer examination of the range of possible fits for **4** (see Table S3) showed that, in fact, a variety of nearly identical fits are possible. All have an Sn−C_α distance of 2.12 Å but have apparent Sn···C distances ranging from 2.76 to 3.03 Å, depending on the starting parameters of the fit. This variability suggested that additional parameters were required to model the data. Consistent with this, the Fourier transform of the fit was not a good match to the data. In particular, the Fourier transform contained a second outer-shell peak, even though only a single Sn···C distance was used in the fit. A better fit was obtained if the Sn···C shell was split into two Sn···C shells (Table S3 and Figure S2, bottom). These fits were robust with respect to starting parameters, consistently giving distances of 2.77 and 3.02 Å. Careful examination of the different contributions to the asymmetric Sn···C fit shows that the two different Sn···C shells have EXAFS contributions that are out-of-phase over much of the range of the data (red and green lines in Figure S2, bottom). The resulting destructive interference means that only a single Sn···C peak is seen in the Fourier transform, although two Sn···C distances are refined. This destructive interference greatly complicates the interpretation of the data.

To test the accuracy of the fit for **4**, EXAFS data were also collected for *n*-$Bu_3Sn^+CB_{11}Me_{12}^-$, whose single-crystal X-ray structure was determined earlier.[10] Because of disorder, the crystallographic data for *n*-$Bu_3Sn^+CB_{11}Me_{12}$ were of low accuracy but nevertheless showed that the tin atom has a distorted trigonal bipyramidal structure, with a Sn−C_α bond length of ∼2.07 Å, and two weak axial Sn···C interactions, with an average distance of 2.81 Å. The Fourier transforms of the EXAFS data for *n*-$Bu_3Sn^+CB_{11}Me_{12}$ and for $Me_3Sn^+CB_{11}Me_{12}$ are compared in Figure 3, together with that for a sample

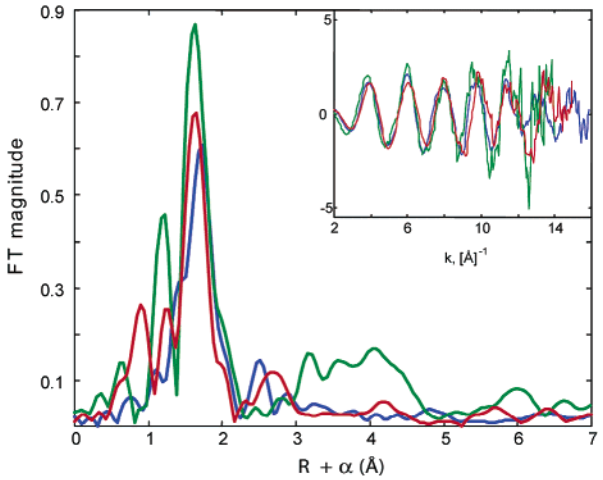

Figure 3. EXAFS (inset) and corresponding Fourier transforms of *n*-$Bu_3Sn^+CB_{11}Me_{12}$ before (blue) and after (green) exposure to air, and for $Me_3Sn^+CB_{11}Me_{12}$ (red).

exposed to air. While the two intact samples have similar Fourier transforms, it is nevertheless clear from a close examination that there are small but significant differences in the Sn environments. The nearest-neighbor Sn−C_α distance in *n*-$Bu_3Sn^+CB_{11}Me_{12}$ is somewhat longer than that in **4**, while the Sn···C distance appears to be much shorter than that in **4**, as indicated by the lower *R* value for the second peak in the Fourier transform. The change in the Sn−C_α distance is confirmed by quantitative fits, which give a value of 2.16 Å (0.04 Å longer than that in **4**, but still close to the usual[70] 2.14 Å Sn−C bond length). The data gave an apparent average Sn···C distance of 2.76 Å, nearly identical to the shorter of the two Sn···C distances in **4** and close to the average Sn···C distance found crystallographically. No longer Sn···C EXAFS signal is seen in *n*-$Bu_3Sn^+CB_{11}Me_{12}$; there is a very small peak that could correspond to a ca. 3.0 Å Sn···C distance, but this peak is near the noise level of the data. The absence of a detectable ca. 3.0 Å Sn···C signal may be due, at least in part, to interference from signals expected from the three C_β carbon atoms in the *n*-butyl chains, located ∼3.0 Å away from the Sn atom. Thus, taking the short Sn···C distance as a measure of pyramidalization, it would appear that the Sn atom in **4** has hybridization very similar to that in *n*-$Bu_3Sn^+CB_{11}Me_{12}$. This is reassuring, given that the ^{119}Sn NMR chemical shifts in the two solids are very similar (466.2 ppm in **4** versus 461.2 ppm[72] in *n*-$Bu_3Sn^+CB_{11}Me_{12}$).

The discrepancy between the Sn−C_α bond length in *n*-$Bu_3Sn^+CB_{11}Me_{12}$ found from the single-crystal X-ray structure,[10] ∼2.07 Å, and the value of 2.16 Å found presently from EXAFS is probably in part due to librational effects and in part due to the low accuracy of the X-ray determination, which was performed on a disordered crystal. We consider the EXAFS value to be the more accurate. In contrast, the two methods agree quite well with regard to the long axial Sn···C distances.

For **6**, the outer-shell Pb···C distance is 2.9 Å, and once again this is accompanied by a very weak distant peak that can be modeled by a linear Pb···C−B interaction. As for **4**, the best fit to this additional interaction gives a reasonable B−C distance of 1.60 Å.[16] Unlike the data for **4**, the data for **6** do not show any evidence for asymmetric Pb···C coordination. The data can

(69) Bondi, A. *J. Phys. Chem.* **1964**, *68*, 441.
(70) Davies, A. G. *Organotin Chemistry*; VCH: Weinheim, 1997.
(71) Batsanov, S. S. *Russ. J. Gen. Chem.* **1998**, *68*, 495.
(72) Zharov, I. Ph.D. Dissertation, University of Colorado at Boulder, 2000; p 53.

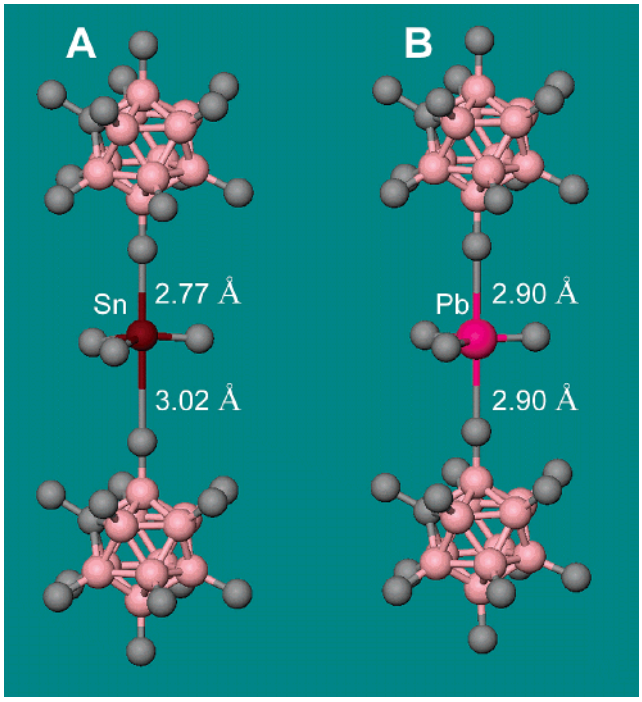

Figure 4. Possible structures of **4** and **6** proposed on the basis of EXAFS results.

be modeled perfectly well assuming symmetric ligation by two Pb···C scatterers at 2.9 Å, and attempts to fit the data using two shells of Pb···C scatterers gave unrealistic negative Debye−Waller factors (Table S3 and Figure S3). It is possible that the failure to resolve two different Pb···C distances in **6** is a result of the shorter *k* range (and thus lower resolution) of the data. However, symmetric ligation by two M···C interactions in **6** would be consistent with apparent increase in M···C distance for **6** and would imply a nearly symmetric, trigonal bipyramidal arrangements for the Me_3Pb^+ cation with rather weak coordination to the two axial methyls provided by the $CB_{11}Me_{12}^-$ anions (Figure 4). Still, it is difficult to rule out entirely the possibility that the Me_3Pb^+ cation has a strongly unsymmetric structure similar to that proposed for Me_3Sn^+. In this case, it is likely that only the shorter of the axial distances is reflected in the EXAFS.

EXAFS of Solid $Me_3Ge^+CB_{11}Me_{12}^-$ (5). The outer-shell scattering is most intense for the germanium compound **5**, which shows two well-defined outer-shell peaks of comparable amplitude. The shorter of these, which appears at ∼ 2.1 Å in Figure 2, is well modeled with a Ge···C distance of 2.49 Å. The EXAFS data would be consistent with either one or two axial interactions at 2.5 Å, representing a distorted tetrahedral and a trigonal bipyramidal structure, respectively. Distinguishing between these two possibilities by EXAFS alone is extremely difficult due to the correlation between the apparent coordination number and the Debye−Waller factor. However, the unusually short axial distance of 2.5 Å is inconsistent with a trigonal bipyramidal structure for the cation in **5**. There is insufficient space around the Me_3Ge plane to permit coordination to two anions, each at 2.5 Å. If the germyl cation had this five-coordinate arrangement, the axial coordination sites would be expected to have significantly longer Ge···C distances. Therefore, a distorted tetrahedral geometry with three short interactions and one long interaction is proposed for the trimethylgermyl cation in **5**. If there were a fifth group coordinated to the germanium atom on the back side, its carbon atom would presumably be much farther than 2.50 Å from the Ge, and probably not detectable by EXAFS.

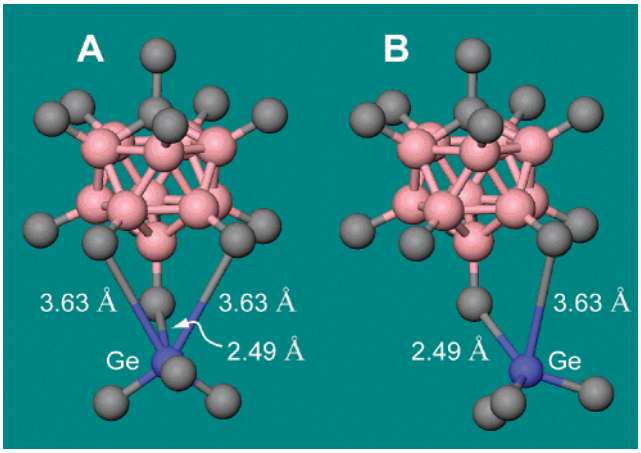

Figure 5. Possible structures of **5** proposed on the basis of EXAFS results.

However, it is clear from Figure 2 that there is another outer-shell peak for **5** at ∼3.1 Å. This peak does not appear to result from a backside methyl group because it is relatively intense. EXAFS amplitudes fall off as $1/R^2$; therefore, given that this peak is nearly 1.5 times as far away, it would be expected to be less than half as intense. Another possible explanation is that this peak is due to a Ge···B interaction from a linear Ge···CH_3—B structure. A linear arrangement would increase the amplitude of the outer-shell EXAFS due to multiple scattering and is probably observed for **4** and **6**, as noted above. However, for **5**, the apparent Ge···B distance (∼3.5 Å) would be too short to be consistent with the observed Ge···C distance and the expected B—C distance. The remaining possibility is to attribute the ∼3.1 Å peak to a shell of Ge···C at an average distance of 3.63 Å, and this can only originate from one or two of the methyls in the associated $CB_{11}Me_{12}^-$ anion (7, or 7 and 8). It requires the Ge−C−B angle to be bent away from 180°, and the absence of linearity in the Ge···CH_3—B moiety then accommodates naturally the absence of detectable Ge···B EXAFS. If the empty metal orbital is pointing in the expected direction, equal tilting toward two methyls (toward a face-centered coordination position on the $CB_{11}Me_{12}^-$ anion) is unlikely due to the resulting short distance (4.0 Å) between at least one of the methyl groups in the Me_3Ge^+ cation and the methyls of the anion (structure A in Figure 5). Such a tilt requires a strong bending with a Ge···CH_3—B angle of 122°. We therefore consider a tilt toward one methyl group (toward an edge-centered coordination position on the $CB_{11}Me_{12}^-$ anion) more likely (structure B in Figure 5, with a 4.7 Å closest distance between the Me_3Ge^+ methyls and those of the anion, and a bending angle of 130°). This tilt produces a five-membered (Ge···CH_3—B—B—CH_3···) ring, which might be rigid enough to give a detectable Ge···CH_3 EXAFS peak at 3.6 Å.

Computations for the $Me_3M^+CB_{11}Me_{12}^-$ Ion Pairs. Although the structures of ion pairs will not be easily related to the structures of the solids, and although interactions other than classical electrostatic forces are not easily calculated with any accuracy between ions of the size in question, we considered it useful to perform calculations on the ion pairs to obtain some insight into the cation−anion interactions in the salts **4**−**6**. First,

Table 2. Calculated (B3LYP/SDD) Energies and Structures of Isolated $Me_3M^+CB_{11}Me_{12}^-$ Ion Pairs

	coordinated methyl group							
	$Me_3Sn^+CB_{11}Me_{12}^-$				$Me_3Ge^+CB_{11}Me_{12}^-$			
	12 (B)	7 (B)	2 (B)	1 (C)	12 (B)	7 (B)	2 (B)	1 (C)
rel *E*, kcal/mol	0	2.4	8.8	20.5	0	2.8	10.0	22.4
q(Me_3M^+), e	+0.74	+0.75	+0.78	+0.82	+0.62	+0.64	+0.70	+0.78
d(M···C), Å	2.42	2.43	2.48	3.07	2.14	2.17	2.25	2.89
d(C−B), Å[a]	1.72	1.71	1.68	1.50[b]	1.85	1.81	1.72	1.50
∠MCB, deg	180	176	171	131	180	177	173	133
$\sum\angle C_\alpha MC_\alpha$, deg	347	348	350	354	340	341	345	353
⟨∠BCH⟩, deg	96	96	99	111[c]	86	89	95	111

[a] Average *d*(C−B) in free **2** is 1.62 Å. [b] *d*(C−C). [c] ∠CCH.

we are interested in the competition among vertex-centered, edge-centered, and face-centered coordination and the relative coordinating ability of the four inequivalent vertex types in the CB_{11}^- cage, and we are looking for guidance concerning the nature of the cation−anion interactions. Second, we compare the interactions with the three different metal cations.

The bulk of our calculations were performed by density functional theory (DFT), a method that describes attractive van der Waals interactions poorly or not at all (Tables 1 and 2). We were only able to afford a calculation by the MP2 method for one of the isomeric ion pair structures of $Me_3Ge^+CB_{11}Me_{12}^-$. This procedure is known to somewhat overestimate attractive van der Waals interactions. In our case, it gives an optimized structure very similar to that obtained from the DFT calculation, except that the incipient S_E2 substitution on the methyl carbon has not proceeded quite as far along the reaction coordinate. This result is reassuring in that it suggests that van der Waals attractions do not play a dominant role in determining the ion pair structure. Nevertheless, while we believe that the results of the computations are quite dependable when it comes to the structure and properties of the individual partner ions, when it comes to inter-ion interactions, they are best viewed as qualitative guides rather than definitive statements.

Relative Coordinating Ability of Methyl Groups in $CB_{11}Me_{12}^-$. Considerable computational effort was expended in a search for potential energy minima in which the cation would be located above a BB edge such as 7−12 or 2−7, or above a BBB triangular face such as 7,8,12. The latter type of coordination is known for the case of toluene−Li^+ [73] and phosphine−Ag^+ [9] salts. No edge-centered or face-centered minima were found in the present case, and in the end, careful geometry optimization always led to one of the minima in which the metal atom lies above a B vertex. This is the type of coordination we concentrate on in the following.

Although many structures of salts of $CB_{11}H_{12}^-$ and its various derivatives have been published over the years, the relative coordinating ability of its inequivalent vertices is somewhat uncertain. Electrophilic interactions with the vertices of $CB_{11}H_{12}^-$ are generally believed to decrease in the reactivity order 12 > 7−11 > 2−6 ≫ 1, but complexes with coordination both through positions 12[74] and 7[42] have been reported. Recently, single-crystal structures of several phosphine−Ag^+ 1-H-$CB_{11}Me_{11}^-$ salts have been described,[8,9] and in some the phosphine-stabilized silver cation is strongly coordinated to a methyl group

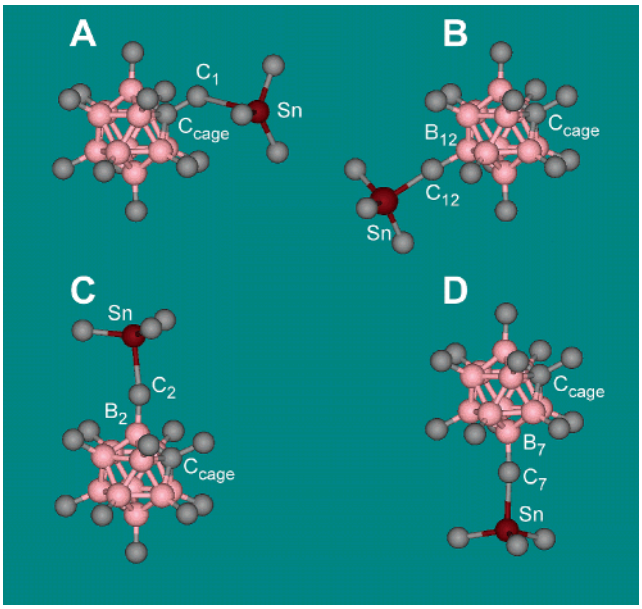

Figure 6. Calculated (B3LYP/SDD) structures of $Me_3Sn^+CB_{11}Me_{12}^-$ ion pairs coordinated to positions 1 (A), 12 (B), 2 (C), and 7 (D) of the $CB_{11}Me_{12}^-$ anion.

in position 7 of the carboranyl anion. Our calculated (B3LYP/SDD) ion-pairing energies of the four separately optimized isomers of an isolated $Me_3Sn^+CB_{11}Me_{12}^-$ (Figure 6) and an isolated $Me_3Ge^+CB_{11}Me_{12}^-$ ion pair with the cation next to positions 1, 2, 7, and 12 favor the association with the 12-methyl group over that with the 7-methyl group, but not by a wide margin (Table 2). The interaction of the cation with the 2-methyl group is considerably weaker. In all three cases, the metal atom prefers to lie almost exactly on the local approximate five-fold axis of the icosahedral anion. In contrast, the cations interact much more weakly with the 1-methyl group, and the metal atom is then tilted off the axial position by nearly 50° toward the 2-methyl group. It is not immediately obvious to what degree these preferences are of purely electrostatic origin and reflect an uneven distribution of charge in the carborane anion (Tables 3 and 4) and to what degree they are due to distinct coordinating abilities of the individual vertices.

Electrostatic Interactions. We consider the classical, purely electrostatic interactions first. These are computed fairly reliably by any of the methods used. The charge distribution in the anions **1** and **2** has been the subject of debate for some years. We have now computed it at the B3LYP/6-31+G(d) level of theory and present the results in Tables 3 and 4, respectively. We list both the natural atomic charges defined by Weinhold[75] and the Mulliken charges; note the vast superiority of the former,

(73) King, B. T.; Noll, B. C.; Michl, J. *Collect. Czech. Chem. Commun.* **1999**, *64*, 1001.
(74) Crowther, D. J.; Borkowsky, S. J.; Swenson, D.; Meyer, T. Y.; Jordan, R. F. *Organometallics* **1993**, *12*, 2897, and references therein.

Table 3. Calculated (B3LYP/6-31+G(d)) Natural[a] and Mulliken Atomic Charges[b] for the Free $CB_{11}H_{12}^-$ Anion (**1**)

	12	7–11	2–6	1
B	−0.161 (−0.077)	−0.185 (−0.046)	−0.022 (−0.047)	−0.712 (−0.651)[c]
H	+0.055 (−0.006)	+0.058 (−0.006)	+0.049 (0.001)	+0.322 (0.224)
vertex[d]	−0.106 (−0.083)	−0.127 (−0.052)	0.027 (−0.046)	−0.390 (−0.427)
Coul attr[e]	−66.07 (−59.51)	−63.45 (−60.33)	−59.04 (−63.52)	−55.25 (−65.03)
elst pot.[f]	−67.06	−64.63	−59.76	−50.69

[a] Reference 66. [b] In elementary charge units; Mulliken charges in parentheses. [c] Cage carbon atom charge. [d] Sum of charges on B (or C) and H atoms at each vertex. [e] Coulombic attraction (kcal/mol) between a +1 point charge, placed 2.5 Å from the hydrogen atom of a vertex on the B−H (C−H) axis, and natural (Mulliken) atomic charges in the anion. [f] Electrostatic potential (kcal/mol) at the point described in footnote *d*.

Table 4. Calculated (B3LYP/6-31+G(d)) Natural[a] and Mulliken Average Atomic Charges[b] for the Free $CB_{11}Me_{12}^-$ Anion (**2**)

	position			
	12	7	2	1
B	+0.102 (−0.757)	+0.065 (+0.408)	+0.253 (+0.880)	−0.548 (−2.063)[c]
C (methyl)	−0.911 (−0.987)	−0.907 (−1.009)	−0.929 (−1.032)	−0.639 (−0.996)
H	+0.236 (+0.206)	+0.236 (+0.205)	+0.241 (+0.211)	+0.243 (0.232)
CH_3	−0.204 (−0.369)	−0.200 (−0.392)	−0.207 (−0.398)	+0.090 (−0.298)
vertex[d]	−0.101 (−1.126)	−0.134 (0.015)	+0.046 (+0.482)	−0.458 (−2.362)
Coul attr[e]	−64.53 (−76.53)	−62.69 (−59.39)	−59.55 (−59.99)	−52.48 (−86.85)
elst pot.	−65.75	−63.96	−59.15	−50.39

[a] Reference 66. [b] In elementary charge units; Mulliken charges in parentheses. Because of the different disposition of the methyl groups at otherwise equivalent vertices, the charges on the latter vary slightly. Average values are given. [c] Cage carbon atom charge. [d] Sum of charges on B, C, and H atoms at each vertex. [e] Coulombic attraction (eV) between a +1 point charge, placed 2.5 Å from the methyl group carbon atom of a vertex on the B−C (C−C) axis, and all natural (Mulliken) atomic charges in the anion.

Table 5. Calculated (B3LYP/SDD) Natural Atomic[a] Charges[b] for Isolated $Me_3M^+CB_{11}Me_{12}^-$ Ion Pairs

		coordinated methyl group							
		$Me_3Sn^+CB_{11}Me_{12}^-$				$Me_3Ge^+CB_{11}Me_{12}^-$			
	position	12	7	2	1	12	7	2	1
CH_3[c]	12	−0.29	−0.33	−0.29	−0.29	−0.25	−0.32	−0.29	−0.28
	7−11	−0.28	−0.28	−0.28	−0.28	−0.27	−0.27	−0.28	−0.28
	2−6	−0.29	−0.29	−0.30	−0.31	−0.28	−0.29	−0.25	−0.31
	1	+0.08	+0.07	+0.05	−0.11	+0.08	+0.07	+0.05	−0.07
vertex[d]	12	−0.05	−0.12	−0.07	−0.06	−0.05	−0.11	−0.06	−0.05
	7−11	−0.14	−0.13	−0.13	−0.13	−0.14	−0.11	−0.13	−0.13
	2−6	+0.14	+0.13	+0.13	0.11	+0.14	+0.13	+0.17	+0.12
	1	−0.67	−0.67	−0.70	−0.89	−0.67	−0.67	−0.70	−0.85

[a] Reference 66. [b] In elementary charge units. [c] Average sum of charges on methyl C and H atoms at each vertex. [d] Average sum of charges on B, C, and H atoms at each vertex.

which reproduce the calculated electrostatic potential at the likely locations of the counterions within a few kilocalories per mole, whereas the latter yield numbers some of which are off by dozens of kilocalories per mole. We use only the former in further discussion. The charges calculated for ion pairs of **2** with Me_3Sn^+ and Me_3Ge^+ remain almost the same regardless of the cation position (Table 5), showing that the anion is not very polarizable and that it is sensible to base the discussion on the charge distribution in the isolated anions.

Two qualitative arguments concerning the charge distribution in **1** and **2** come to mind. At first sight, the general tendency of positive counterions to associate with positions 7−12 in the known crystal structures and the preponderance of electrophilic substitution in these positions suggest that most of the negative charge is located in positions distant from the cage carbon atom. Yet, one would expect the most electronegative atom in the cage, the carbon in position 1, to carry most of the negative charge.

The charges listed in Tables 3 and 4 neatly resolve this apparent contradiction. In agreement with the relative electronegativities of carbon and boron, in the free $CB_{11}H_{12}^-$ anion (**1**)[76] most of the calculated negative charge resides on vertex 1, which carries 3 times the negative charge of the most negative boron vertex. Vertices 2−6 are nearly electroneutral. Each single vertex in the group 7−12 is weakly negative, but together, they carry about three-fourths of a negative elementary charge. Interestingly, vertex 12 is slightly less negative than vertices 7−11. Within each vertex, the charge is distributed unevenly. The hydrogens in positions 2−12 are weakly positive, and the negative charge on these vertices is carried by the boron. Together, the boron atoms in positions 7−12 carry little over 1 unit of negative charge. The carbon-bound hydrogen in position 1 is positive (and is also known to be fairly acidic).

In the $CB_{11}Me_{12}^-$ anion (**2**), the charge distribution among the vertices is similar, with the carbon vertex 1 even more strongly negative. The 1-methyl group is nearly electroneutral, whereas the 2−12 methyls are strongly and equally negative. The positive charges on the boron atoms, large negative charges on the methyl carbons, and positive charges on the methyl hydrogens remind us that, on boron, methyl is a σ-withdrawing and π-donating substituent.

(75) *NBO*, Version 3.1: Glendening, E. D.; Reed, A. E.; Carpenter, J. E.; Weinhold, F. Reed, A. E.; Curtiss, L. A.; Weinhold, F. *Chem. Rev.* **1988**, *88*, 899.

(76) (a) Zahradník, R.; Balaji, V.; Michl, J. *J. Comput. Chem.* **1991**, *12*, 1147. (b) McKee, M. L. *J. Am. Chem. Soc.* **1997**, *119*, 4220.

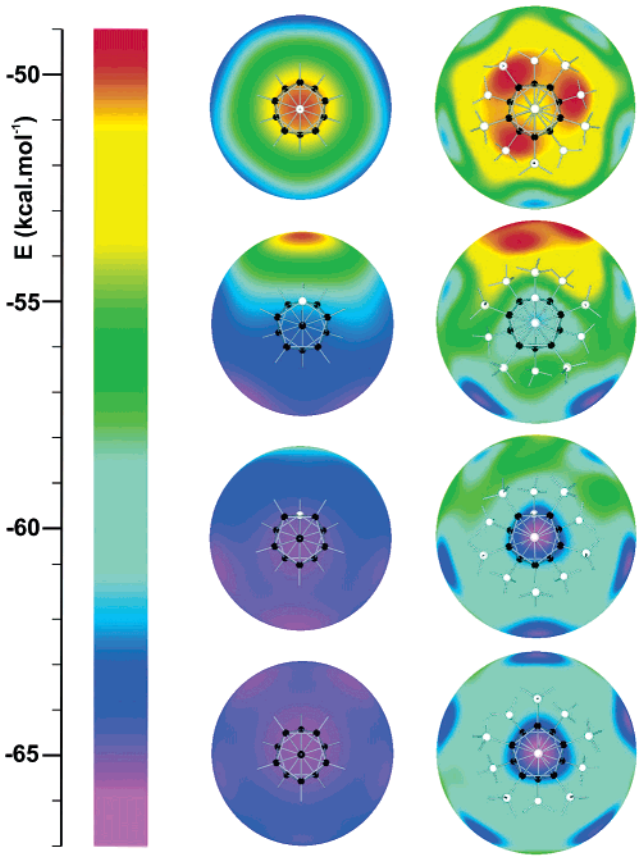

Figure 7. Sphere: Electrostatic potential (B3LYP/6-31+G(d)) around $CB_{11}H_{12}^-$ (**1**, left) and $CB_{11}Me_{12}^-$ (**2**, right). The radii of the spheres are 5.2 and 5.7 Å, respectively, 2.5 Å from the hydrogen atoms (**1**) or methyl carbon atoms (**2**). Views along exocyclic bonds; from top to bottom, looking at positions 1, 2, 7, and 12.

Thus, in both cases, vertex 1 carries not only close to half of all the negative charge but also a significant local dipole whose positive end is pointed outward. This makes it difficult for a positive counterion to derive much stabilization from interaction with the negative charge on the carbon vertex by approaching it closely, and it is better off when located at the opposite end of the cage. This becomes clear when all Coulombic interactions between the cation and the anion are added quantitatively. This can be done crudely by adding pairwise interactions between atomic point charges calculated by the Weinhold procedure, or accurately by computation of the electrostatic potential, with similar results (Tables 3 and 4). The relative preferences are not very different in **1** and **2**.

The electrostatic potentials around **1** and **2** calculated for the surfaces of spheres of a radius appropriate for the Me_3Sn^+ counterion are presented in Figures 7 and 8. These graphical presentations provide a particularly instructive picture of the strong deviation of the electrostatic potential around these anions from spherical symmetry. In both instances, a clear preference is given to the location of the positive point counterion in position 12, closely followed by those in positions 7−11, and distantly by positions 2−6 and particularly 1.

Covalent Interactions. The calculated structures of the partner ions leave little doubt that there is more to the interaction than mere electrostatics. The presence of true chemical bonding interactions in the computed structures is not in doubt for the isomers in which the cation is located in positions 2−12, as

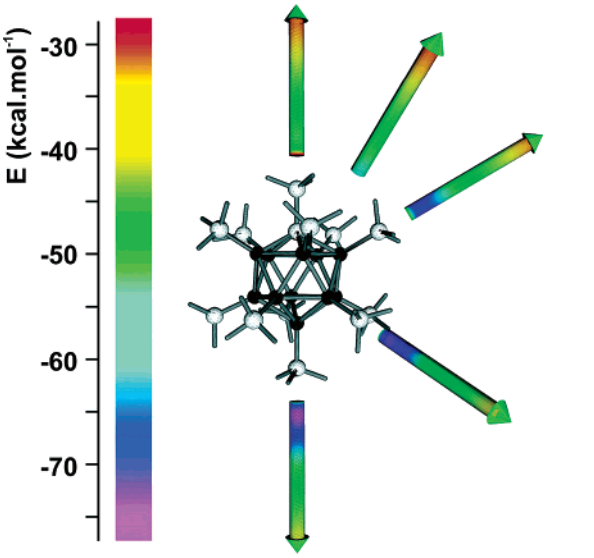

Figure 8. Electrostatic potential (B3LYP/6-31+G(d)) around $CB_{11}Me_{12}^-$. The 5 Å long color-coded arrows are placed 1.2 Å above the carbon atom of methyl groups in positions 1, 2, 7, and 12. One arrow is placed between positions 1 and 2, showing that in this region the electrostatic potential is higher than that directly above the methyl group in position 1.

the B−C bond at the vertex adjacent to the cation Me_3Sn^+ (Me_3Ge^+) is 0.1 Å (0.2 Å) longer than the others, the coordinated methyl group is flattened, and the cation is distinctly pyramidalized (Table 2). The geometrical distortions calculated for the interaction of the cations with the 1-methyl group of the anion are quite different. Compared to the other isomers, the M···C distance is much bigger (for Ge, by ∼0.7; for Sn, by ∼0.6 Å), the cage−CH_3 bond is only slightly stretched (by 0.02 Å), the methyl group remains tetrahedral ($\sum\angle$HCH is smaller by ∼31° for Ge and ∼36° for Sn), and the Sn^+ center is less pyramidalized ($\sum\angle C_\alpha MC_\alpha$ is larger by ∼11° for Ge and ∼6° for Sn). The Me_3M^+ group is tilted toward the methyl in position 2 ($\angle$CCGe = 133°, $\angle$CCSn = 131°), whereas for the other three isomers the metal atom M lies in a direction very close to that of the B−C bond at the vertex. The computed degree of electron density shift from the anion to the cation is much less in the 1-methyl isomer than in the others.

The calculated geometrical distortions suggest that the covalent interaction is of the type expected if the cation interacted with the carbon atom of the methyl groups in positions 2−12, and with two of the hydrogen atoms of the methyl group in position 1. When the 12, 7, and 2 isomers of the Me_3Ge^+ or Me_3Sn^+ ion pairs are compared, those with the cation in position 12 have the shortest M···CH_3 and the longest B−CH_3 distance, the most pyramidalized Me_3Sn^+ cation, the flattest methyl group, and the most inter-ion charge transfer (Table 2). Judging by the nature of the geometrical distortions, the empty orbital of the metal atom removes electron density from the back lobe of carbon orbital that is used to attach the methyl group to the cage boron atom. In contrast, the interaction between the metal cation and the 1-methyl group seems to involve the CH bonds of the methyl.

The purely electrostatic and the covalent energetic preferences thus coincide, and both favor position 12, followed by 7, 2, and 1. A comparison of the relative DFT energies of the four isomeric $Me_3Sn^+CB_{11}Me_{12}^-$ and $Me_3Ge^+CB_{11}Me_{12}^-$ ion pairs (Table 2) with the relative energies of the purely electrostatic

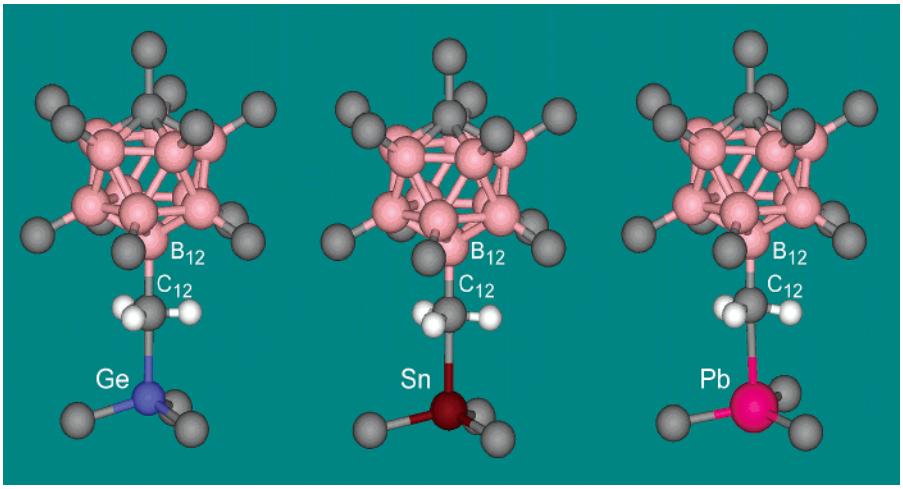

Figure 9. Calculated (MP2/6-31G(d) and B3LYP/SDD) structures of $Me_3M^+CB_{11}Me_{12}^-$ (M = Ge, Sn, Pb) ion pairs with coordination to the methyl group in position 12 of the carborane.

interactions (Table 4) suggests that the electrostatic effects are responsible for two-thirds to three-fourths of the preference and the covalent effects for the rest.

Relative Coordinating Ability of the Metal Atoms in Me_3M^+. A comparison of the DFT optimized structures computed for the ion pairs **4**, **5**, and **6** is provided in Figure 9 and Tables 1 and 2. The most notable results are the following: (a) the M···CH_3—B arrangement is nearly linear; (b) the cations are pyramidalized and the coordinating 12-methyl group of the anion is flattened; (c) the B(12)−C(12) bond of the anion is elongated; and (d) the M···C(12) distance is much longer than in normal covalent M—C bonds but much shorter than the sum of van der Waals radii of the metal and of a methyl group. The structural distortions from the free ion structures are calculated to diminish in the series Ge, Sn, Pb. This is also the order of decreasing inter-ion charge transfer (Table 2) and agrees with the conclusion drawn from the solid-state ^{13}C NMR chemical shifts, namely that the positive charge on C_α increases in the series of Me_3Ge^+, Me_3Sn^+, and Me_3Pb^+. The calculated structure of $Me_3Ge^+CB_{11}Me_{12}^-$ seems to be approaching the transition-state geometry for backside S_E2 substitution on the carbon of the CH_3 group.

The MP2 calculated structure of $Me_3Ge^+CB_{11}Me_{12}^-$ is very similar to that described above, but the B(12)−C(12)−Ge angle is 171°, the germyl cation is less pyramidalized, and the B(12)−C(12) bond is less extended, as if the intended S_E2 substitution on the methyl carbon were somewhat less advanced. The methyl group coordinated to the germyl cation is still essentially planar, as would be expected in the transition state.

Comparison of the Computed Structures of Ion Pairs 4−6 with the EXAFS Structures of Solids (Table 1). The computed structures of the ion pairs are not easily extrapolated to the solid structures. In addition to the purely electrostatic interactions with the other ions present, in the solid both the anion and the cation are capable of specific interactions with more than one counterion, as suggested by the published[10] crystal structure of *n*-$Bu_3Sn^+CB_{11}Me_{12}^-$. As expected, the calculated M−C(12) distances in the ion pairs are much shorter than those found by EXAFS for the solids **4**, **5**, and **6**. Optimization on the ion triple $[CB_{11}Me_{12}^-Me_3Sn^+CB_{11}Me_{12}^-]$ with coordination through positions 2 and 9 (equivalent to 7) of the anion (Figure 10) at the B3LYP/SSD level resulted in a structure with the three

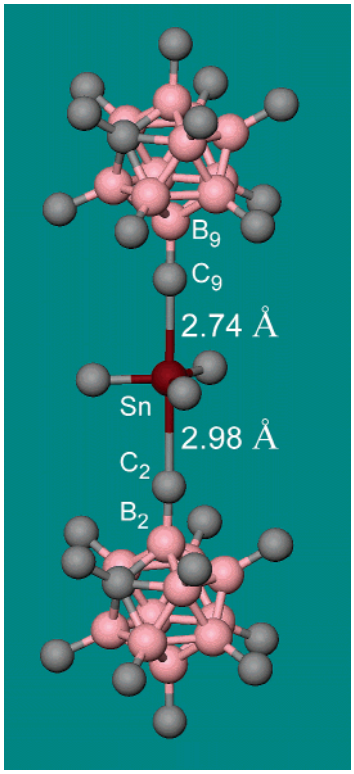

Figure 10. Calculated (B3LYP/SDD) structure of the $[CB_{11}Me_{12}^-Me_3Sn^+CB_{11}Me_{12}^-]$ ion triple.

constituents nearly coaxial. The two inequivalent Sn···C distances are 2.74 Å (9-Me) and 2.98 Å (2-Me), now in nearly perfect agreement with observations on the solid (Table 1). The cation is calculated to be pyramidalized less than observed in the crystal of *n*-$Bu_3Sn^+CB_{11}Me_{12}^-$ (Sn atom 0.08 Å out of the C_α plane; observed, 0.32 Å). This is in line with the conclusion drawn above from the EXAFS results.

Except for the obvious difference in the Sn−C_α and Pb−C_α bond lengths, well reproduced by the calculations, the Me_3Sn^+ salt **4** and the Me_3Pb^+ salt **6** are calculated and observed to be very similar (Table 1). Overall, EXAFS of $Me_3Sn^+CB_{11}Me_{12}^-$ (**4**) and $Me_3Pb^+CB_{11}Me_{12}^-$ (**6**) suggests that, in these solid, each cation is coordinated to two anions in infinite columns similar to those found in the single crystal of *n*-$Bu_3Sn^+CB_{11}Me_{12}^-$.[10]

In that case, assuming additivity of the coordination energies, our calculations suggest that it is energetically more favorable by 10.6 kcal/mol for the cations to coordinate to the antipodal positions 2 and 9 of the anion, rather than the antipodal positions 1 and 12, even if it leaves the best coordinating methyl group in position 12 unused. Although the calculations are for ion pairs and observations for a solid lattice, the trends in the two are similar. The distance from the metal to the carbon of the coordinated methyl group is computed to be ~0.2 Å longer in the Pb-containing free ion pair than in the Sn-containing free ion pair. The difference of the distances observed in the solid is a little over 0.1 Å (counting the closer methyl group in **4**).

While the EXAFS results for the outer shells in **4** and **6** are very similar, there is no doubt that the structure of Me_3Ge^+-$CB_{11}Me_{12}^-$ (**5**) is quite different. Instead of forming an unsymmetrical trigonal bipyramid, the Me_3Ge^+ cation is coordinated primarily to one and more weakly to one (or, less likely, two) other methyl group of a single anion. Our calculations suggest that, in a free ion pair, the germanium would prefer coordination to a single methyl group on an anion, but in the solid it is apparently advantageous to coordinate to two; in that case the primary coordination is expected to be to position 12, and the weaker coordination to position 7. We have no information on how these ion pairs pack into the solid lattice. The very noticeable observed reduction in the Ge···CH_3 distance relative to Sn···CH_3 (by ~0.3 Å) and Pb···CH_3 (by 0.4 Å) is quite nicely reproduced by the calculations and suggests that the coordination of the Me_3Ge^+ cation is much stronger than that of Me_3Sn^+ and Me_3Pb^+. Presumably, this provokes a much stronger pyramidalization at the Ge^+ atom and sterically precludes any stabilizing coordination from its back side.

Experimental Part

General. Standard Schlenk and glovebox techniques were used for handling air-sensitive reagents. Pentane, hexane, cyclohexane, methylcyclohexane, benzene, Me_6Si_2, Me_6Sn_2, Me_6Ge_2, and Bu_6Sn_2 were dried over CaH_2, distilled, and stored under Ar. The solvents were stored over a potassium mirror. The following compounds were purchased and used as received: Ph_4Ge, Ph_4Sn, Ph_4Pb, Me_3SnPh, PhLi, *t*-BuLi, ethyl triflate, calcium hydride, cesium chloride, and silver nitrate. $Me_3NH^+CB_{11}H_{12}^-$ was purchased from Katchem Ltd. (Prague, Czech Republic). Solution ^1H, ^{11}B, ^{13}C, ^{29}Si, ^{119}Sn, and ^{207}Pb NMR spectra were measured with Varian XRS-300 and Varian Unity-500 spectrometers. ^1H and ^{13}C chemical shifts were measured relative to the lock solvent. ^{11}B chemical shifts were measured relative to BF_3OEt_2, with positive chemical shifts at higher frequency. $B(OCH_3)_3$ was used as an external standard (18.1 ppm). ^{29}Si, ^{119}Sn, and ^{207}Pb chemical shifts were measured relative to the corresponding Me_4E. Solid-state CP/MAS ^{11}B, ^{13}C, and ^{119}Sn NMR spectra were obtained on a Chemagnetics CMX-200 spectrometer using a Chemagnetics MAS probe equipped with a 7.5 mm PENCIL rotor. Due to the air sensitivity of the compounds, the samples were sealed in short sections (approximately 15 mm) of 5 mm o.d. tubing. These tubes were then packed into the rotor surrounded by KBr to aid in balancing of the samples for high-speed spinning. Spin rates between 1 and 2.5 kHz were attained. The ^{11}B spectra of the three different salts (**4**, **5**, **6**) were all identical; therefore, no effort was made to properly reference these spectra. The ^{13}C spectra were externally referenced using HMB, with the methyl resonance being 17.6 ppm on the TMS scale. The ^{119}Sn spectrum was referenced using the signal from tetracyclohexyltin, with the Sn resonance taken to be −97.4 ppm on the $SnMe_4$ scale.[77] Attempts to measure the ^{207}Pb chemical shift in the Pb complex were not successful. Mass spectra were recorded with a Hewlett-Packard 5989 API/ES/MS. An HPLC system employing a reverse-phase C_{18} column (250 × 4.6 mm, 5 μm) with methanol/water (containing a 1% AcOH/0.7% Et_3N buffer) as the mobile phase was used for monitoring reactions, while larger columns of the same phase were used for semipreparative separations. All volatile compounds were analyzed using Varian 3400 analytical GC with a 0.2 mm × 25 m, 0.33 μm RSL-150 5% cross-linked silica capillary column. Their separations were performed using Varian 3400 preparative GC with a $^1/_4$ in. × 21 ft 5% OV-7 80/100 Chromosorb GHP packed column. Individual compounds were purified to >99.5% purity (by analytical GC).

EXAFS Experiments. All carborane species were synthesized and sealed under a dry argon atmosphere until use. Tetraphenylmetal compounds were purchased from Aldrich and used without further purification. Sample powders were ground with dry BN and packed evenly into a 1 mm thick sample cell with polypropylene windows. All sample manipulation was performed in a glovebox under a dry nitrogen atmosphere.

X-ray absorption data were collected at Stanford Synchrotron Radiation Laboratory (SSRL). Data collection details are summarized in Table S1 (see Supporting Information). Absorption data were collected in transmission mode using N_2-filled ion chambers for Ge and Pb, and Ar-filled ion chambers for Sn. X-ray energies were calibrated using an element foil as an internal standard, with the first inflection point of the foil defined as 11 103 (Ge, K-edge), 26 714 (Sn, K-edge), or 13 038 eV (Pb, L_3-edge). A Si (220) double-crystal monochromator was used in all cases.

Data were analyzed using EXAFSpak, written by G. N. George at SSRL. Averaged absorbance data were processed using a second-order polynomial pre-edge subtraction, a k^3-weighted, four-region, third-order spline for extended X-ray absorption fine structure (EXAFS) background removal, and were scaled using a Victoreen background function. The EXAFS formula used for data fitting is

$$\chi(k) = \sum_{i=1}^{n} \frac{N_i F_i(k,r) S_i(k)}{kr^2} \sin(2kr + \phi_{tot})$$

where N_i is the number for scatterer i at the distance of r to the photoabsorber, $F_i(k,r)$ is the backscattering amplitude, $S_i(k)$ is a scale factor, ϕ_{tot} is the total phase shift of the scattering path, and the sum is over all types of scattering atoms.

EXAFS data were fitted using amplitude and phase parameters calculated with FEFF 7.02, and calibrated using EXAFS data for $GePh_4$, $SnPh_4$, and $PbPh_4$ (Table S2, Supporting Information), which gave for the element threshold energies of 11 113.5 (Ge), 29 213.6 (Sn), and 13 036.8 eV (Pb). The scale factor was held constant at 0.9. These parameters gave accurate first-shell fitting (see Table S2). These E_0 values and scale factor were used to fit the k^3-weighted data for the carborane compounds. The bond distance and the Debye−Waller factor for each shell were optimized until the square sum of the k^3-weighted differences between raw data and the FEFF model reached minimum. The bond-valence sum (BVS) analysis[78] was applied to each optimization result as an accessory tool to choose the best fit. The bond valence (s) is defined as

$$s = \exp\left(\frac{r_0 - r}{B}\right)$$

where $B = 0.37$, r is the bond length, and r_0 is an empirical value. For a given metal ion, the BVS is the sum of bond valences for each bond pair to the metal ion. The empirical value of r_0 was determined to minimize the difference between the BVS and the formal oxidation

(77) Harris, R. K.; Sebald, A. *Magn. Reson. Chem.* **1987**, *25*, 1058.

(78) Brown, I. D.; Altermatt, D. *Acta Crystallogr.* **1985**, *B41*, 244.

state for crystallographically characterized compounds from the Inorganic Crystal Structure Database (ICSD).

Calculations. Geometry optimizations were performed using the Gaussian 98 program,[79] charges were calculated using the NBO method,[75] and molecular modeling and visualization were performed using Molden 3.6[80] and Spartan SGI Version 4.1.1 (Wavefunction, Inc). The basis sets used were SDD (i.e., D95V for H, B, and C, and Stuttgart/Dresden ECPs for Ge, Sn, and Pb),[81] 6-31G(d),[82] and 6-31+G(d).[82]

All structures have been optimized with increased integral precision (Int = UltraFine) up to tight convergence. For all resulting geometries the Hessian matrices were analyzed, and if negative eigenvalues appeared, the geometry was changed until all eigenvalues remained positive and the geometries corresponded to true potential energy minima. For each of the four isomers of both Me_3Ge^+ and Me_3Sn^+ salts, the optimization was started from three different geometries, with the cation placed against the B−CH_3 (C−CH_3) vertex, between two adjacent vertices, and between three adjacent vertices. In all cases, the geometries converged to the same structure. In six of them (three for Me_3Ge^+ and three for Me_3Sn^+), the cation ended up placed against essentially exactly against a boron vertex, with the B−C−M angle nearly exactly equal to 180°. Only for the isomers with the Me_3Ge^+ or Me_3Sn^+ cation located in position 1 was the C−C−M line significantly bent, with the metal atom inclined away from its carbon vertex and toward one of the adjacent B−CH_3 vertices.

Data for electrostatic potential plots were obtained from the Gaussian cube file.

Oxidation with $CB_{11}Me_{12}^{\bullet}$—General Procedures. The $CB_{11}Me_{12}^{\bullet}$ radical is placed in a flame-dried ampule equipped with a stir bar and a septum. The ampule is connected to a dry solvent reservoir and to a vacuum/Ar line by thick-walled latex tubing. The system in evacuated (10^{-3} mmHg), the vacuum line is disconnected, and the desired amount of solvent is distilled into the ampule cooled in liquid nitrogen. The system is then filled with argon, and the solution is warmed to the desired temperature with stirring until all radical is dissolved. A material to be oxidized is added dropwise with vigorous stirring either neat (dry, degassed) using a syringe or as a dry, degassed solution in an alkane solvent via a Teflon cannula. After the blue (pentane, hexane) or green (cyclohexane, methylcyclohexane) color of the radical disappears, the reaction is complete. Trapping reagents are added to the resulting solution/solids via a syringe or a cannula. For further sample preparations, the solvent can be carefully removed from insoluble products via cannula, or evaporated in the case of soluble products, after which the ampule can be sealed. Solid-state NMR samples were prepared by opening ampules in a glovebox, transferring their contents into an NMR tube equipped with a vacuum connector, and sealing the tubes, first off the vacuum line and then to the desired length on a lathe. EXAFS samples were prepared in a glovebox by grinding the salts with dry BN powder and packing the mixture evenly into a 1 mm thick sample cell with polypropylene windows.

(79) Frisch, M. J.; Trucks, G. W.; Schlegel, H. B.; Scuseria, G. E.; Robb, M. A.; Cheeseman, J. R.; Zakrzewski, V. G.; Montgomery, J. A., Jr.; Stratmann, R. E.; Burant, J. C.; Dapprich, S.; Millam, J. M.; Daniels, A. D.; Kudin, K. N.; Strain, M. C.; Farkas, O.; Tomasi, J.; Barone, V.; Cossi, M.; Cammi, R.; Mennucci, B.; Pomelli, C.; Adamo, C.; Clifford, S.; Ochterski, J.; Petersson, G. A.; Ayala, P. Y.; Cui, Q.; Morokuma, K.; Malick, D. K.; Rabuck, A. D.; Raghavachari, K.; Foresman, J. B.; Cioslowski, J.; Ortiz, J. V.; Stefanov, B. B.; Liu, G.; Liashenko, A.; Piskorz, P.; Komaromi, I.; Gomperts, R.; Martin, R. L.; Fox, D. J.; Keith, T.; Al-Laham, M. A.; Peng, C. Y.; Nanayakkara, A.; Gonzalez, C.; Challacombe, M.; Gill, P. M. W.; Johnson, B. G.; Chen, W.; Wong, M. W.; Andres, J. L.; Head-Gordon, M.; Replogle, E. S.; Pople, J. A. *Gaussian 98*, revision A.9; Gaussian, Inc.: Pittsburgh, PA, 1998.

(80) Schaftenaar, G.; Noordik, J. M. *J. Comput.-Aided Mol. Design* **2000**, *14*, 123.

(81) H, B, C: Dunning Jr., T. H.; Hay, P. J. In *Modern Theoretical Chemistry*; Schaefer, H. F., III, Ed.; Plenum: New York, 1976; Vol. 3, pp 1−28. Ge, Sn, Pb: Igel-Mann, G.; Stoll, H.; Preuss, H. *Mol. Phys.* **1988** *65*, 1321.

(82) H, C: Hehre, W. J.; Ditchfield, R.; Pople, J. A. *J. Chem. Phys.* **1972**, *56*, 2257. B: Dill, J. D.; Pople, J. A. *J. Chem. Phys.* **1975**, *62*, 2921. +: Clark, T.; Chandrasekhar, J.; Schleyer, P. v. R. *J. Comput. Chem.* **1983**, *4*, 294. d: Hariharan, P. C.; Pople, J. A. *Theor. Chim. Acta* **1973**, *28*, 213.

$Me_3Sn^+CB_{11}Me_{12}^-$ (4) was prepared at room temperature as a white solid in 20 mL of pentane from 25 mg (0.08 mmol) of the $CB_{11}Me_{12}^{\bullet}$ radical and 8.4 μL (13.2 mg, 0.04 mmol) of Me_6Sn_2 in 97% yield (37 mg). CP-MAS ^{11}B NMR: δ −1.7 (B_{12}), −11.8 (B_{2-11}). CP-MAS ^{13}C NMR: δ 57.5 (1-C), 14.4 (1-CH_3), 10.4 (CH_3−Sn), −1.5 (2−12-CH_3). CP-MAS ^{119}Sn NMR: δ 466.8. IR (solid): 582, 687, 773, 869, 950, 1068, 1143, 1247, 1285, 1365, 1461, 2846, 2865, 2939 cm^{-1}. MS/ES(+) in methanol: base peak at *m*/*e* 165 with the expected isotopic distribution (Me_3Sn^+). MS/ES(−) in methanol: base peak at *m*/*e* 311 with the expected isotopic distribution ($CB_{11}Me_{12}^-$). Anal. Calcd for $C_{16}H_{45}B_{11}Sn$: C, 40.45; H, 9.55. Found: C, 40.97; H, 8.99.

The ^{119}Sn and ^{11}B NMR spectra of **4** in C_6D_6, CD_2Cl_2, and CD_3CN were obtained by preparing **4** in an NMR tube in pentane under argon atmosphere, removing pentane, adding the dry deuterated solvent, and sealing the tube. For low-temperature NMR measurements, the sample preparations were conducted at −78 °C, and the sealed and frozen NMR tubes were transported to an NMR instrument.

An analogous reaction of 25 mg (0.08 mmol) of the $CB_{11}Me_{12}^{\bullet}$ radical and 15.8 μL (18.8 mg, 0.08 mmol) of Et_4Sn in 20 mL of pentane resulted in a white solid after 1 h of stirring at room temperature. ES/MS of this solid in methanol showed a base peak at *m*/*e* 206 (positive mode) with the expected isotopic distribution (Et_3Sn^+), and base peak at *m*/*e* 311 (negative mode) with the expected isotopic distribution ($CB_{11}Me_{12}^-$). A small peak at *m*/*e* 325 (negative mode) was also detected ($CB_{11}Me_{11}Et^-$).

$Me_3Ge^+CB_{11}Me_{12}^-$ (5) was prepared at room temperature as a white solid in 20 mL of pentane from 25 mg (0.08 mmol) of the $CB_{11}Me_{12}^{\bullet}$ radical and 8.0 μL (9.4 mg, 0.04 mmol) of Me_6Ge_2 in 96% yield (33 mg). CP-MAS ^{11}B NMR: δ −1.5 (B_{12}), −11.6 (B_{2-11}). CP-MAS ^{13}C NMR: δ 57.6 (1-C), 14.4 (1-CH_3), 5.6 (CH_3−Ge), −1.7 (2−12-CH_3). IR (solid): 605, 707, 775, 879, 955, 1078, 1145, 1248, 1295, 1369, 1463, 2844, 2867, 2931 cm^{-1}. MS/ES(+) in methanol: base peak at *m*/*e* 119 with the expected isotopic distribution (Me_3Ge^+). MS/ES(−) in methanol: base peak at *m*/*e* 311 with the expected isotopic distribution ($CB_{11}Me_{12}^-$). Anal. Calcd for $C_{16}H_{45}B_{11}Ge$: C, 44.79; H, 10.57. Found: C, 45.21; H, 10.09.

An analogous reaction of 25 mg (0.08 mmol) of the $CB_{11}Me_{12}^{\bullet}$ radical and 15.2 μL (15.1 mg, 0.08 mmol) of Et_4Ge in 20 mL of pentane resulted in a white solid after 2 h of stirring at room temperature. ES/MS of this solid in methanol showed a base peak at *m*/*e* 160 (positive mode) with the expected isotopic distribution (Et_3Ge^+), and a base peak at *m*/*e* 311 (negative mode) with the expected isotopic distribution ($CB_{11}Me_{12}^-$). A small peak at *m*/*e* 325 (negative mode) was also detected ($CB_{11}Me_{11}Et^-$).

$Me_3Pb^+CB_{11}Me_{12}^-$ (6) was prepared at room temperature as a white solid in 20 mL of pentane from 25 mg (0.08 mmol) of the $CB_{11}Me_{12}^{\bullet}$ radical and 17.0 μL (21.5 mg, 0.08 mmol) of Me_4Pb in 93% yield (42 mg). CP-MAS ^{11}B NMR: δ −1.5 (B_{12}), −11.6 (B_{2-11}). CP-MAS ^{13}C NMR: δ 57.6 (1-C), 31.4 (CH_3−Pb), 14.7 (1-CH_3), −1.8 (2−12-CH_3). IR (solid): 542, 667, 778, 867, 952, 1062, 1145, 1246, 1285, 1366, 1462, 2843, 2867, 2933 cm^{-1}. MS/ES(+) in methanol: base peak at *m*/*e* 253 with the expected isotopic distribution (Me_3Pb^+). MS/ES(−) in methanol: base peak at *m*/*e* 311 with the expected isotopic distribution ($CB_{11}Me_{12}^-$). Anal. Calcd for $C_{16}H_{45}B_{11}Pb$: C, 34.10; H, 8.05. Found: C, 34.66; H, 7.75.

Conclusions

The oxidation of Me_6E_2 (M = Ge, Sn) and Me_4Pb with $CB_{11}Me_{12}^{\bullet}$ in pentane yields the insoluble salts Me_3M^+-$CB_{11}Me_{12}^-$, which have been characterized by chemical trapping, NMR, EXAFS, and calculations. In these solids, the cationic lead or tin center is coordinated to the methyl groups of two $CB_{11}Me_{12}^-$ anions in a trigonal bipyramidal fashion, the former most likely symmetrically and the latter unsymmetrically. The cationic germanium center is coordinated strongly to one

and weakly to another one or two methyls of a single $CB_{11}Me_{12}^-$ anion. Most of the interaction is electrostatic, but a quarter to a third can be attributed to covalent bonding. The strength of the metal−methyl interaction increases in the order $Me_3Pb^+ < Me_3Sn^+ \ll Me_3Ge^+$, and the strength of both the electrostatic and covalent interaction increases in the position order $1 \ll 2 < 7 < 12$. Electrostatic potential plots for $CB_{11}H_{12}^-$ and $CB_{11}Me_{12}^-$ on the surface of a sphere centered at the center of the icosahedron clearly display a deviation from spherical symmetry.

When the methyl is carried by a boron atom, the associated metal cation behaves as if it were attempting a backside S_E2 substitution on the methyl carbon; when it is Me_3Ge^+, it nearly succeeds in reaching the transition state for extraction of the methyl group. When the cation is Me_3Si^+ or Me_3C^+, the transfer of the methide anion actually succeeds.[49,72] In these cases, we propose that the coordinative bonding interaction is best represented by a dotted line between the metal atom and the carbon of the "methidic" methyl group, since its hydrogens play a secondary role and are actually pushed aside by the metal ion. When the methyl is carried by a carbon, its interaction with the metal ion is quite different and primarily involves two of the methyl hydrogens.

Acknowledgment. This work was supported by the National Science Foundation (CHE-0140478 and CHE-9709195) and by the Ministry of Education of the Czech Republic (Center for Complex Molecular Systems and Biomolecules, project LN00A0032). The EXAFS data were measured at SSRL, a national user facility operated by Stanford University on behalf of the U.S. Department of Energy, Office of Basic Energy Sciences, with additional support from the Department of Energy, Office of Biological and Environmental Research, and the National Institutes of Health, National Center for Research Resources, Biomedical Technology Program.

Supporting Information Available: Full experimental details for all new compounds. This material is available free of charge via the Internet at http://pubs.acs.org.

JA0475205